Paleoseismology of the oblique-normal Ekkara Rupture Zone (April 30, 1954 M 6.7-7.0 Thessaly earthquake, Greece) - archaeological and geochronological constraints on ground rupture recurrence

N. Palyvos[(1)], K. Pavlopoulos[(1)], E. Froussou[(2)], H. Kranis[(3)], K. Pustovoytov[(4)], S.L. Forman [(5)], D. Minos-Minopoulos[(3)]

In press at the Journal of Geophysical Research (AGU), available on-line in the "papers in press" section: http://www.agu.org/journals/pip/jb/2009JB006374-pip.pdf

(This document is the same version as in the link above, not containing proof print corrections)

(1) Harokopio University, Department of Geography, El. Venizelou 70, Athens, Greece.

(2) 14th Ephorate of Prehistoric and Classical Antiquities, Kastro Lamias, Lamia, Greece.

(3) University of Athens, Faculty of Geology and Geoenvironment, Panepistimioupolis Zografou, 15784 Athens, Greece.

(4) University of Hohenheim, Institute of Soil Science and Land Evaluation , Emil-Wolff-Str. 27, 70599 Stuttgart, Germany.

(5) University of Illinois at Chicago, Luminescence Dating Research Laboratory, 845 West Taylor Street (M/C 186), Chicago, Illinois 60607-7059, U.S.A.

Abstract

Observations in trenches excavated across the Ekkara rupture zone (ERZ), the longest of the sporadic ground ruptures that accompanied the M 6.7-7.0 earthquake of April 30, 1954 on the Domokos fault zone (DFZ), identify a left-lateral oblique-normal fault with a slip vector aligned with the regional extension direction (verifying the tectonic origin of the ERZ). The paleoseismological interpretation of stratigraphic, soil-stratigraphic and tectonic features is discussed with emphasis on the issues related to strongly oblique fault kinematics. Two pre-1954 events of ground rupture are recognized (E1 and E2) and, an event of ground cracking only (E1a, shortly after E1). Event E2 was accompanied by larger displacement than E1 and 1954, this not necessarily implying a stronger earthquake though.

Archaeological dating of transported ceramic sherds constrains E1 between 6750-4450 BP (more likely, 6450-5750 BP). Luminescence dating of colluvial deposits and ^{14}C dating of pedogenic carbonates (stone coatings), place E2 at ~17500 +- ~2500 BP (preferred age). In the (hazard-wise) most conservative interpretation, recent recurrence intervals of ERZ activations exceed 3195 yr.

The sporadic nature of the 1954 ruptures precludes certainty on whether the ERZ has recorded *every* past activation of the DFZ, unless data are collected also from other DFZ rupture zones. Minimum-limiting estimates of 0.3-0.5 mm/yr slip rate are derived for the ERZ, true slip rate expectedly not exceeding 1 mm/yr. Slip rate estimates for the ERZ may be minima for the DFZ though, because co-seismic deformation in the past may have been distributed to more than one rupture zones at the surface.

Key words: ***Paleoseismology, Oblique-slip normal fault, Holocene recurrence interval, Domokos fault zone, Ekkara rupture zone, April 30 1954 "Sofades" earthquake, Thessaly (Greece).***

Introduction

Surface faulting (ground ruptures) during moderately strong (M 6.5-7.0) earthquakes can be complex and/or sporadic in areas of multi-fractured upper crust, such as Greece [e.g. *Pavlides*, 1993]. If in addition, deformation rates are slow, complex ground rupture zones can have a geomorphic expression that is very subtle (due to long repeat times of surface faulting events), and they can thus be difficult to identify based on surface observations alone. More so, in areas where their expression may be obscured by man-made geomorphological features resulting from human activities that span several millennia (as in Greece and elsewhere). In such cases, documented co-seismic ground ruptures are invaluable for guiding trenching paleoseismological studies [e.g. *McCalpin and Nelson* 1996; *Yeats et al*., 1997].

The April 30, 1954 "Sofades earthquake" in Thessaly [*Papastamatiou and Mouyiaris*, 1986; *Ambraseys and Jackson*, 1990] (Figure 1a/b), occurred in a multi-fractured setting [*Pavlides*, 1993], and was accompanied by sporadic and locally complex ground ruptures. The 1954 earthquake is probably the strongest documented earthquake in Thessaly, with a magnitude estimated between 6.7 [*Ambraseys and Jackson*, 1990] and 7.0 [*Papazachos and Papazachou*, 2002; *Papadimitriou and Karakostas*, 2003]. It apparently marked the onset of an eastward-migrating sequence of strong (Mw>6.2) earthquakes along the southern margin of the Thessaly region, all the way to Volos (V in Figure 1b) [e.g. *Papastamatiou and Mouyiaris*, 1986; *Papadimitriou and Karakostas*, 2003].

The historical seismicity record for Thessaly is certainly incomplete prior to A.D. 1621, and generally does not allow for reliable association of historical earthquakes with a specific fault zone [*Papadopoulos*, 1992; *Caputo and Helly*, 2005]. The only information available for the 1954 seismogenic fault zone in specific, is that it apparently has not given a 1954-like earthquake in the past 200 to 300 years [*Papadopoulos*, 1992; *Caputo et al.*, 2006] - Figure 1b. Thus, if we are to obtain information about past earthquakes on this fault zone, paleoseismological or archaeoseismological studies are required.

This paper regards the results of a trenching paleoseismological study on the largest of the ground rupture zones that were observed along the 1954 fault zone. We present the stratigraphic, soil-stratigraphic (pedological) and tectonic features in three closely spaced trenches, followed by a discussion of their paleoseismological interpretation that emphasizes the problems related to the strongly oblique kinematics of the trenched rupture zone. The results of and the issues involved in multidisciplinary efforts for the dating of recognized paleoseismic events are also discussed. The timing of the penultimate event of ground ruptures is determined by archaeological dating of transported ceramic sherds. Optical dating of colluvial sediments and radiocarbon dating of pedogenic carbonate coatings (rinds) on cobbles are employed to constrain the timing of the pre-penultimate event. Subsequently, the first conclusions that can be reached regarding the seismic behavior of the 1954 fault zone are summarized, with mention of the limitations that the multi-fractured context of the 1954 earthquake poses in the generalization of paleoseismological results from one ground rupture zone only to the entire 1954 fault zone.

Active-tectonic and geomorphological context of the study site

The 1954 seismogenic fault zone (the 1954 "earthquake segment", *sensu DePolo et al.*, 1991), called the "Domokos fault zone" (DFZ; *Caputo*, 1995), is a major normal fault zone that defines the southern boundary of the western Thessaly plain. It extends between areas 1 and 2 in Figure 1c [*Ambraseys and Jackson*, 1990; *Caputo and Pavlides*, 1993; *Pavlides*, 1993; *Caputo*, 1995], having a clear geomorphic expression at broad scales of observation (those of Figures 1b/c). At least locally, the definition of distinct geomorphic segments is also possible [e.g. *Valkaniotis*, 2005; *Palyvos and Pavlopoulos*, 2008]. However, the 1954 ground ruptures were sporadic (including ruptures of gravitational origin) and locally complex, reflecting control by discontinuities of the inherited, pre-neotectonic structure [*Caputo and Pavlides*, 1993; *Pavlides*, 1993].

The longest of the 1954 ground rupture zones, the Ekkara Rupture Zone (ERZ, at Ekkara village; Figure 1d). trends NNW-SSE for 3.45 km, obliquely to the main geomorphic trace of the DFZ, paralleling a pre-neotectonic discontinuity. Upon reaching the DFZ range front piedmont, the ERZ changes to a NW-SE general strike, similar to the general strike of the DFZ. It crosses the apex of a Holocene alluvial fan, and continues along the ophiolite bedrock / alluvium contact until point A in Figure 1e (a spring), west of which the 1954 ruptures died out. Farther West, ground ruptures appeared at location K and near Gavrakia (Figure 1d) [*Ambraseys and Jackson*, 1990; *Palyvos and Pavlopoulos*, 2008].

The area where the ERZ crosses the alluvial fan is a geomorphic / sedimentary environment that was considered promising for trenching paleoseismological investigations. Here, Upper Holocene deposits are present and adequate deposition rate for the preservation of paleoseismic evidence is expected. Also, in this area it was possible to find a site subjected to minimal post-1954 human modification of the ground surface (Figure 1f). Abundant ceramic sherds found during field reconnaissance at the surface of a deeply ploughed field just North of the trench site (location B in Figure 1e), and an archaeological layer rich in ceramic tiles

and animal bones that outcrops just upslope of the ruptures (location C in Figure 1e), indicated that transported archaeological material useful for dating faulted Holocene deposits could be expected also in the trenches. .

Field data collection

Field reconnaissance to locate the exact trace of the ERZ was undertaken, based on the map of *Papastamatiou and Mouyiaris* [1986] and interviews with eye-witnesses of the 1954 ground ruptures. A reconnaissance trench followed by three trenches (T1-3) were excavated by backhoe at the same location (Figure 2). The trenches were studied using variations of standard techniques described by *McCalpin* [1996a]. Detailed topographic survey of the trench site was carried out, in order to precisely position the trenches with respect to each other. Trench walls were scraped clean, gridded at irregular horizontal and vertical intervals, and photographed. Image warping software was used for on-site construction of photo-mosaics, 1:10 or larger scale printouts of which were used for detailed logging of stratigraphic, tectonic and soil-stratigraphic (pedological) contacts and locations of archaeological and other samples. The ~5m deep single-slot reconnaissance trench was not logged because it was re-filled and expanded to become T1 soon after its excavation and partial cleaning, for safety reasons. The walls of T1 and T2 were left to weather for several months and were revisited several times. At key locations, trench walls were progressively cut back by hand up to six times, to clarify ambiguous stratigraphic and tectonic features. Kinematic indicators on the main fault plane and secondary splays were measured at several locations. Sampling of materials for dating included transported archaeological ceramic sherds, colluvial sediments for optical dating and samples of pedogenic carbonate (stone coatings) for ^{14}C dating.

Trench stratigraphy and soil stratigraphy

The units depicted in the logs (Figures 3 to 5) are lithostratigraphic units, including also particle size and sedimentologic structure changes due to pedogenesis (soil formation). Lithostratigraphic units whose distinguishing lithofacies characteristics are the result of pedogenesis have pedogenic lower boundaries, whereas their upper boundaries may be either pedogenic or erosional. Lithostratigraphic units with different codes in different trenches or different trench walls can be equivalent chronostratigraphically, as shown in Figure 6. In the following, references to units without a sub-unit modifier refer also to all of the sub-units (where present). E.g., "U7" refers to the entire package that sub-units U7a, b, c and d make together and, "U7b" collectively refers to U7b1, 2 and 3. A lithostratigraphic unit may contain sediments deposited by different processes. E.g., Unit 5 consists of stream channel deposits in its lower part, but its upper part locally includes colluvium derived from these deposits (see paleoseismological interpretation). Units drawn with a pattern of thick horizontal lines, indicate uncertainty in correlation with neighbouring units (line colors indicate the alternative interpretations).

Holocene deposits

The fault zone (the ERZ) juxtaposes peridotite bedrock (BR and wBR) with Holocene colluvial and alluvial deposits (Figures 3 to 5, and 7a/b). Unit descriptions are given in Figure 4, with additional information in the sections discussing the tectono-stratigraphic and archaeological evidence. For further details and trench wall photomosaics, see *Palyvos and Pavlopoulos* [2008].

Colluvial deposits include scarp-derived colluvium [e.g. *Schwartz and Coppersmith*, 1984, *Nelson*, 1992] (e.g. U8, U7) and, colluvium from the far-field slope (e.g. U1a on the upthrown fault block). Both types of colluvium may be present in a given colluvial unit.

Alluvial deposits derive both from the Mazi R. (Figure 2f) and smaller streams on the Mazi alluvial fan surface. Alluvium from the Mazi R. possibly dominates U9, judging from the presence of abundant rounded cobbles within U9 in T3. Overbank deposits from the Mazi R. could be present also at the distal part of scarp-derived colluvial wedges (e.g. within U7 at the distal part of T1 and T3) and also within the colluvial deposits on the upthrown block, but they are indistinguishable. Unit 1b could be a mudflow deposit from the Mazi R., or colluvium containing stones from man-made constructions uphill of the trenches (a similar stone/boulder layer is found at location C in Figure 1e). Deposits from smaller streams include bedload-dominated deposits (U2, not associated to a distinct paleochannel, and U1d / U5, in paleochannels 1 / 2, resp.; Figure 8), and overbank deposits (U5d, associated with paleochannel 2).

Erosional surfaces

Five erosional surfaces were identified within the Holocene deposits (ES1 to ES5 in Figure 8). The erosional nature of the above surfaces was directly identifiable in some cases, e.g. by the angular unconformity between U2 and U4/7 at the SE wall of T1. However, the entire picture given in Figure 8 is based also on indirect arguments stemming from the

tectono-stratigraphic interpretation. Except for ES1, the erosional surfaces are displaced and rotated by the ERZ. Erosional surface ES4 is the product of fault scarp erosion after an event of ground rupture (see tectono-stratigraphic interpretation). Question-marks indicate two alternative traces of ES2 close to fault C (the lower trace being more likely). In this area the limit between U3 and U2 was indistinct, hence the question-marks and dotted lines in Figure 3a. Unit 4b (T1, SE wall), which is a part of U4 that is characteristically rich in large pebbles, might overlie an erosional surface (ES3). ES3 is purely inferential, based on the tectono-stratigraphic interpretation in the following, and could be the product of human activity, considering that there seems to be no –obvious- explanation for a natural origin. The upper boundary of the bedrock probably corresponds to an initially sub-horizontal erosional surface (ES6), which is also deformed by the ERZ (and possibly re-eroded, close to the main ERZ strands).

Buried calcic soil horizons

Two buried "Bk" (calcic) paleosoil horizons with carbonate morphologies [e.g. *Birkeland*, 1999] were encountered in the trenches (Bk1 and Bk2, drawn with white hatch patterns in the logs).

In T1 (SE wall), Bk1 consists of a lower, well-developed part on U7b and U6 (Figure 9g), typified by $CaCO_3$ precipitates predominantly within planar veins but also as irregularly shaped concretions around root passages or pebbles. The upper part of Bk1 occupies U5 and the lower part of U4, with generally less developed carbonate morphologies (an exception being U4c; Figure 7b). The upper part of Bk1 on the SE wall of T1 is not drawn with hatch pattern in the log for legibility reasons and, because it's upper limit was generally indistinct. On the NW wall of T1, Bk1 (U7b) was not sub-dividable in a lower and upper part

In T2, Bk1 consists of well-developed lower part (on U7b, with similar morphology as in T1) and an upper part characterized by faint, thin veins (on U5a, c and d, probably also the lower part of U4; only the part on U5d is shown in Figure 4). In T3, Bk1 is also composite. It's upper sub-horizon (on U7b1) consists of thin planar veins (Figure 5c). These veins extend also into U7b2, the upper part of the lower Bk1 sub-horizon in T3, which consists of a 30-65 cm thick horizon of thicker, more irregularly shaped, friable $CaCO_3$ deposits (Figure 5c/e) compared to U7b1. The lower part of the lower Bk1 sub-horizon (on U7b3), has a diffuse limit with the upper part (on U7b2), corresponding to a progressive decrease of $CaCO_3$ deposits.

The pedogenic discontinuity between the lower and upper part of Bk1 in T1 (SE wall) and T2 (both walls) corresponds to a change in sedimentation rate that is not related to a paleoearthquake but, to the establishment of paleochannel 2 along the ERZ. In contrast, the similar discontinuity in Bk1 in T3 is the result of "tectonic burial" of the lower Bk1 sub-horizon [*sensu West,* 1993] – see paleoseismological interpretation and Figure 6.

The lower Bk horizon (Bk2, developed on U9) was exposed in T1 and T3. In T1 it had a minimum thickness of 1.3 m, and consisted of thicker, less regularly shaped veins compared to Bk1 (Figures 3d and 10b). Vein concentration was apparently higher at the upper part of the horizon. Laterally non continuous, thin caliche (about 1 cm thick or less) was observed also along the upper bounding surface of the Bk horizon, which was very sharp and planar, indicating a possible erosive surface (Figure 10b). This possible erosive surface was absent a few meters away from the fault zone in T1 and was nowhere observed in T3. This lack of lateral extent, together with the lack of any visible difference in the sedimentary facies of units 7 and 9 (if Bk2 is put aside, that is), suggests that the –possible- erosive surface in T1 should not correspond to an important hiatus.

In T3, the upper boundary of Bk2 was more irregular and indistinct (i.e. no signs of it being erosive as in T1). Also, Bk2 morphology was different, being dominated by up to 8-9 cm thick sub-horizontal layers of soft $CaCO_3$ deposits mixed with fine-grained U9 sediment (Figures 5c and 10c). In T3, U9 contained rounded cobbles and small boulders (Figure 10c), on which $CaCO_3$ coatings (or cutans, or rinds – e.g. *Chadwick et al.*, 1989; *Pustovoytov*, 2002 and references therein) up to 1 cm thick were observed.

The fault zone

The ERZ consists of a main fault plane (labeled "A") on the relatively healthiest (hardest) bedrock in the trenches, which has a moderate dip (38-43^o) in T2 and T3, where the ERZ strikes NW-SE, and becomes steeper (54-57^o) at the more NNW-SSE-striking stretch of the ERZ in T1, which was excavated across a small-scale relay zone (Figure 1e). In all trenches, secondary, steeper faults (labeled "B") splay from fault A at different depths. These faults dip 60-70^o and strike oblique to fault A (stereoplots in Figure 2), bounding intensely crushed, sheared and softened bedrock (wBR) in its hanging-wall block. The wBR occurrences appear as wedges in vertical cross-section, and are observed at different length scales. The B faults that bound them probably have curved traces in horizontal section, suggesting that the wBR wedges correspond to lenses in 3-D. In T2, secondary, B-equivalent faults without any wBR on their footwall are also observed (faults L and G), the wBR wedge and associated B fault lying deeper in the downthrown block. The steeper, secondary faults are those generally associated with the largest discrete

displacements of Holocene deposits. The main fault A is buried by Holocene deposits in T1, and in T3, it has hosted smaller displacements than faults B. In T2 (SSE wall) though, also the upper part of fault A has hosted appreciable recent displacement.

At several locations [details in *Palyvos and Pavlopoulos*, 2008], kinematic indicators (striations) were found on fault A and the B splay faults (e.g. Figure 7d, measurements plotted in Figure 2). All striations found at the deeper parts of fault A (T1 and T2 only) show sinistral (left-lateral) oblique displacement, with an important horizontal component (given as percentage of vertical displacement in Figure 2). The strike-slip component of displacement is largest in T1, in agreement with the location of T1 in a relay zone. Oblique slip characterizes also all measured B faults, as well as the B-equivalent fault L in T2 (SSE wall). In T2, on the higher part of fault A, higher than the rooting point of B-equivalent faults (L and G), dip-slip striae were identified on fault A1, indicating gravitational sliding of the wedge between B-equivalent faults and the main fault plane A. The slip vectors derived in the trenches are in very good agreement with the direction of active extension determined by *Caputo and Pavlides* [1993] (Figure 2), thus verifying that the 1954 rupture along the ERZ was tectonic.

Interpretation of tectono-stratigraphic features

The determination of paleoearthquake "event horizons" [*Pantosti et al.*, 1993], in the following is making use of those tectono-stratigraphic and pedogenic features that were most clear. Ambiguous features are also discussed and accounted for in the proposed interpretation. Because of the important horizontal component of displacement, as in strike-slip faults [e.g. *Weldon et al.*, 1996], vertical stratigraphic separations (VSSs) may be smaller or larger than the respective fault throw (or even of opposite sense), depending on the apparent dip of stratigraphic contacts in a direction parallel to the strike of the fault. In the following, VSS differences between successive contacts are evaluated in this respect before true differences in vertical displacement (throw) are inferred.

The 1954 rupture

According to detailed eye-witness accounts of the 1954 rupture, the height of the scarp free face (the vertical separation of the ground surface) was about 70 cm in the area of T1, increasing to 1 m towards T2. The VSS of units 1b and 2 in both T1 and T2 are consistent with the above, indicating that U1b and U2 have experienced the 1954 rupture only. In T3, discrete vertical separation was smaller, and/or distributed to more fault strands at the surface (T3 NW wall).

Colluvium from the 1954 scarp was generally not distinguishable within U1. On the SE wall of T1, the thickening of U1b at the downthrown block resembles a wedge of debris element scarp-derived colluvium [*Nelson*, 1992] but, it is merely the result of horizontal translation juxtaposing thicker and coarser U1b on the downthrown block, against a thinner and finer part of U1b on the upthrown block.

The penultimate event (E1)

Trench 1

A first line of evidence for the penultimate event (E1) comes from fault F (Figure 7c/b), which showed up during progressive cut-back of the bench separating the upper and lower parts of the SE wall of T1. Fault F affects the lower part of U5 (including U5b; Figure 7b) and is covered by a lush $CaCO_3$ coating without identifiable striae (Figure 7e). In sharp contrast, fresh striae from the 1954 slip are found on a thin clay film over fault A (main fault plane) and on faults H1/H2 (small anastomosing faults right in front of A), which are in addition completely $CaCO_3$-free. These features suggest that fault F formed during a pre-1954 event (E1) that took place before pedogenic $CaCO_3$ deposition ceased. Based on the upward extent of fault F, the event horizon of E1 lies somewhere above U5b. The lower part of U5 was clearly back-tilted in the immediate hangingwall area of fault F. This deformation has not affected the base of U4, indicating that E1 predates U4.

Event E1 is evidenced also from increase in VSS moving from U1/U2 to U5. Figure 3e summarises on-fault and "far-field" VSS measurements. "Far-field" is used in an informal sense, that of measuring away from the internal complexity of the fault zone, to the extent the wall dimensions allow. Far-field measurements require planar stratigraphic markers (e.g. the base of U1b, or the top of paleochannel 2), to avoid misinterpreting elevation differences caused by pre-existing relief (e.g., the case of the base of U4). On-fault VSS of U5b, is similar to the far-field VSS obtained from all of paleochannel 2 (Figure 3e/f). These values are more than twice the VSS of U1b (55 cm on-fault, less than ~59 cm far-field). Considering the small dip component of the bases of U1b and U5 in a direction parallel to the fault zone, this VSS difference is large enough to correspond to true difference in cumulative throw.

The debris element of scarp-derived colluvium from event E1 corresponds to the part of U5a filled with a checkered pattern in the interpreted logs in Figure 8. This is suggested by: (a) the conspicuous thickening of

U5a towards the fault zone, (b) the homogeneity of this part of U5a, in contrast to more distal parts of U5a, where bedding was clear, at least locally, and (c) the unconformity between the base of U4 (dipping to the NE) and the base of U5a (back-tilted to the SW). The debris wedge does not have an identifiable contact with the underlying sediments (i.e. the lowest, alluvial part of U5a above U5b). Lack of a sharp basal contact of the debris wedge can be attributed to: (a) the rupture occurring within the active channel of a stream, where reworking of debris was taking place, and (b) most of the scarp free face consisting of U5. Material from U5b and perhaps also U7b can explain the increased amount of fines in the debris wedge.

The next youngest unit after E1 is U4, a colluvium that deposited on the sloping surface of the E1 debris wedge and is interpreted as the "wash element" of the E1 colluvial wedge, i.e. the colluvium that deposited after the complete burial of the scarp free face [*Nelson*, 1992]. The basal contact of U4 was sharp, as is often the case with bases of wash element colluvium [*McCalpin*, 1996b]. Unit 4 lacks a typical wedge-like shape due to: (a) its lateral transition to U3, (b) possible erosion during its deposition (ES3 in Figure 8) and, (c) erosion after it's deposition (ES2).

Unit 4 interfingers with U3, which had markedly different texture and was characteristically poorer in ceramic sherds compared to U4. Interfingering and textural contrast suggest that U3 and U4 contain sediment arriving from different transport directions and source areas, respectively. The gentle NE general apparent dip and the thinning of U3 away from the fault, suggests colluvial provenance, i.e. either scarp-derived colluvium (related to E1), or colluvium from the far-field slope arriving at the scarp crest.

On the NW wall of T1, where U4 and U5 were absent, no sedimentary, tectonic or pedological evidence of event E1 were identifiable within U7. This can be the result of both (a) lateral die-out of the E1 rupture or of the associated vertical separation of the ground surface (due to the pre-faulting topography) and, (b) E1 forming a scarp where only U7 was exposed (not the bedrock below it). Considering the homogeneous and fine composition of U7, the debris element of colluvium from a scarp on U7 only would expectedly be difficult to distinguish from U7 on the downthrown block, considering also that the post-E1 deposits were subjected subsequently to soil formation. Another possible factor that might also be involved is that an important part of the fault displacement may have been slow (afterslip, as in 1954 at nearby locations along the Ekkara rupture – *Papastamatiou and Mouyiaris*, 1986; *Palyvos and Pavlopoulos*, 2008), i.e. that the co-seismic displacement did not form a free face high enough to produce distinguishable debris facies colluvium in the type of deposits at hand.

An estimate of ~74 cm VSS from E1 (T1, SE wall) is obtained by subtracting the "far-field" VSS of U1b (1954 slip only) from that of paleochannel 2. Considering the gentle NW dip of paleochhannel 2 between T1 and T2, and the sinistral sense of strike-slip displacement, VSS should be somewhat smaller than true vertical displacement. Given the uncertainties involved, what we may say is that about 74(+) cm of VSS compares well to the vertical separation observed in 1954, and generally suggests an earthquake of similar magnitude.

Minor features on the SE wall of T1 allow for the possibility of a second event (E1a) of very little slip or of ground cracking only, soon after E1 took place. Such a feature is a small fissure on the top of U5a exactly above the hinge of the back-tilted part of U5, i.e. on the debris wedge of E1. Lack of VSS of the top of the E1 debris wedge, suggests cracking rather than displacement. Features potentially relevant to E1a are the small displacements of the U4 base by the possible small antithetic faults Y, which do not affect the top of U4. However, this may well be the result of upward die-out [*Bonilla and Lienkaemper*, 1990] of faults that formed in 1954. Important -lateral- die-out was indeed observed at fault X, which before about 20 cm of wall cut-back was associated to about 13 cm of offset of the U4 base. Also, fault C (1954 slip only) was not discernible as a continuous fault in the initial trench wall, but as two en echelon strands with diffuse terminations, the lower strand terminating within U4. Another feature, the small increase of on-fault VSSs across faults B and C together, moving from the base of U1b (55 cm) down to the base of U4 and U5a (61 and 64 cm, resp. - Figure 3e), can also be attributed to 1954 slip, since is explainable by horizontal displacement of stratigraphic contacts that are not perfectly planar and parallel.

Trench 2

On both walls of T2, the differences of on-fault separations of the bases of U1b and U4 are negligible (see log restorations in Figure 4f and g). Because these contacts have a small dip component parallel to the fault strike, negligible separation differences indicate negligible difference in displacement, thus placing event E1 before U4.

On the SSE wall, a marked difference in the amount of warping of the base of U1b and of bedding surfaces within U5c against fault A/A1 (Figure 4c), place E1 above the lower part of U5. So does the remanent VSS of the base of U5 across A1 in Figure 4f, because very clear, fresh striae found on A1 indicate pure dip-slip in 1954. Therefore, this remanent VSS cannot be the result of horizontal displacement during 1954, i.e. a pre-1954 event (E1) is necessary.

Fault G, which hosted the largest discrete displacement in 1954, is associated with a small amount of VSS of the base of U5 and a pronounced

mismatch of U5 lithofacies across it (Figure 4a). This is due to the combination of (a) the horizontal component of displacement, (b) the geometry of paleochannel 2 (U5c and alluvial part of U5a) in map view and, (c) the nature of U5a on the downthrown block of fault G. As far as (c) is concerned, the specific part of U5a was more homogeneous compared to alluvial parts of U5a, and it's top was dipping away from the fault (see restored log in Figure 4f). These features suggest that U5a on the downthrown block of fault G is most likely the debris element of the scarp-derived colluvial wedge associated to E1. The configuration we see today, with coarse paleochannel 2 deposits missing on the downthrown block of fault G, is due to the geometry of paleochannel 2 in map view (reconstruction in Figure 2), in combination with the horizontal component of displacement. Horizontal displacement has juxtaposed part of the main channel (U5c and most of the undifferentiated part of U5 on the upthrown block of G) with overbank fines (U5d on the downthrown block). The lack of remanent VSS of the base of U5d across fault G in the restored log in Figure 4f, suggests that fault G was probably not involved in E1.

Fault B does not affect the base of neither U1b nor U4, i.e. it did not slip in 1954. It has apparently affected the upper part of U7b though, indicating that it participated in E1. Difficulty in identifying unit boundaries above fault B did not permit us to ascertain whether fault B was associated with minor displacement of the base of U5a during E1a (discussed later on).

On the NNW wall, the restored log (Figure 4g) shows clearly the top of U5a dipping away from the fault zone area. This geometry, together with the homogeneity and increased fine-grained content of U5a, agrees with it being E1 scarp-derived colluvium as interpreted on the SSE wall of T2 and the SE wall of T1. Slip during E1 was distributed in the closely spaced faults S, P and Q, which are associated with discrete steps of the base of U5c. $CaCO_3$ accumulations along these faults indicate that calcic soil formation continued after E1. A minimum value for vertical separation during E1 can be obtained from the thickness of the associated colluvial wedge (U5a and U4), which is about 70 cm. This value is minimum thickness because the colluvial wedge is truncated by erosional surface ES2 (Figure 8). The NNW wall also reveals that in T2, the abrupt soil-stratigraphic change between the lower and upper part of Bk1 (U7b and U5d/U5a+c, resp.) does not correspond to tectonic burial [*sensu West*, 1993]. I.e. it did not result from increase of sedimentation rate on the fault hangingwall due to activation of the ERZ, but due to.the establishment of paleochannel 2 (U5) along the ERZ (Figure 6).

The NNW wall of T2 gives the strongest evidence of a secondary, post-E1 paleo-event of ground cracking (event E1a). A V-shaped fissure was observed along fault P on U5a in the initial wall instances. This fissure was dying out towards the NW, as shown by 5 wall cut-backs. Unit 5a in this area being interpreted as post-E1 colluvium, the fissure on it needs to correspond to a post-E1 deformation event (E1a). The lower part of the fissure fill consisted of material from U5a, and the upper part was U4d, which in one wall instance was quite richer in ceramic sherds and animal bones than the rest of U4 in T2 (i.e., U4d could be man-made fill). As shown in the restored log in Figure 4g, as in T1, also here we cannot assign more than a few cm of slip to event E1a, at best. Evidence of E1a are found on the SSE wall also, where a possible small V-shaped fissure was observed on the U5a debris wedge against fault G (Figure 4d). A well-defined fissure was observed also along fault H on the SSE wall (Figure 4c/d). The fissure started appearing after the 2nd cut-back and, together with fault H it was progressively rotating counter-clockwise in successive wall instances. We attribute fissure formation to E1a and it's rotation, as well as most of the VSS of U4 across fault H, to slip in 1954.

Event E1a may correspond to minor slip during a strong E1 aftershock, or sympathetic slip [*sensu DePolo et al.*, 1991] during an earthquake on a nearby fault, soon after E1 on the DFZ. The 1954 earthquake did trigger a cascade of large earthquakes on nearby faults [e.g. *Papadimitriou and Karakostas*, 2003], but ground cracking along the ERZ was not observed during those earthquakes.

Trench 3

In T3, the VSS of the base of U1 on fault B was small, of the order of 35-50 cm (Figure 5a/b). The base of U1 was found at similar elevations on both walls, i.e. its dip component parallel to the fault strike is small. Therefore, VSS in this case is close to true vertical displacement. Small vertical displacement indicates that true slip was small and thus, that horizontal displacement was even smaller (74% of vertical displacement, in T3). A small horizontal displacement in 1954 should not produce dramatic difference between VSS and true vertical displacement on older contacts that have been subjected to the 1954 slip only. Thus, retrodeformation of the trench log, which is generally problematic when a strike-slip component of displacement is involved [e.g. *McCalpin*, 1996a], is in this case useful, in conjunction with other evidence, for the identification of pre-U1 contacts that have been displaced only in 1954.

On the SE wall of T3, removing the 1954 VSS on fault B, the base of U7a is perfectly restored (Figure 5f). On the NW wall of T3, restoration is less perfect (Figure 5g), but the observed small mismatches of the top and bottom of U7a across fault T are within the possible error involved in tracing the top of U7a (very diffuse in this area) and, in any case explainable as differences in stratigraphic separation caused by

horizontal translation of contacts not perfectly horizontal in a direction parallel to the strike of the fault. The full restoration of the base of U7a after removal of the 1954 slip, suggests that U7a has been displaced only in 1954. The "far-field" elevation change of the base of U7a as well as its thickening across fault B, are not the result of displacement that took place after U7a started to deposit, but of the morphology of the ground surface that U7a covered (a smoothed-out pre-existing scarp, formed by E1).

On the NW wall of T3, the continuity of U7b2, a well-developed sub-horizon within Bk1, is clearly not restored after removal of the 1954 stratigraphic separation (Figure 5g). The 1954 displacement being small, it is unlikely that the important remanent mismatch of U7b2 across fault B is due to horizontal displacement in 1954. This suggests that E1 took place after the soil formation that produced the part of Bk1 that corresponds to U7b2. Erosion of U7b2 near fault B at the upthrown block, one of the soil catena phenomena described by *McCalpin and Berry* [1996] in multi-event fault scarps, agrees with the above interpretation.

As the restorations in Figure 5f/g indicate, close to fault B, on both walls, the base and top of U7b2 had a more or less strong initial dip component to the NE. In contrast, the top of U9 is back-tilted (to the SW), as the base of U1 and U7a are, only more. This clearly suggests that the NE dip of U7b2 is not the product of deformation, but, the result of soil formation on a sloping surface. Based on examples of colluvial deposition and soil formation on fault scarps [e.g. *Nelson*, 1992; *West*, 1993; *McCalpin and Berry*, 1996; *Birkeland et al.*, 1991 in *McCalpin*, 1996a], and the evidence identifying the next older event E2 (next section), we infer that the soil formation that produced the part of Bk1 that corresponds to U7b2 (and U7b3), occurred on the sloping surface of the colluvial wedge associated with event E2.

Faulting by E1 created accommodation space for more colluvial deposition at the downthrown fault block, and resulted in tectonic burial [*sensu West*, 1993] of the lower Bk1 sub-horizon (U7b2/3). Unit 7b1 is the deposit right above the event horizon of E1, and presumably consists of colluvium derived from the scarp that E1 formed. Within U7b1, lithofacies that could be interpreted as the debris element of post-E1 scarp-derived colluvium were not identifiable. The explanation for this may involve all the factors involved in the lack of E1 signature on the NW wall of T1 (excluding lateral die-out of the E1 ground rupture). The fact that U7b1 does not thicken towards the fault (unlike an "ideal" colluvial wedge), has to do with the gradient of the pre-faulting surface. Whereas colluvium on faulted sub-horizontal ground surfaces thickens towards the fault, colluvium deposited on faulted sloping surfaces of earlier wedges (the E2 wedge in our case) results to be thinner and less wedge-shaped [*McCalpin*, 1996b, p. 120, ref to *Ostenaa*, 1984]. The fact that U7b1 has been subjected to calcic soil formation is in keeping with the results in T1 (SE wall) and T2, which indicate that soil formation continued after E1. Unit 7a is the part of the post-E1 colluvial wedge that deposited after soil formation stopped (Figure 6) due to non-tectonic causes. That is, we consider that the entire post-E1 colluvial wedge consists of U7b1 and U7a together. This wedge possesses the atypical attribute of a buried soil *within* it rather than *on its top*, because soil formation ceased during wedge deposition.

Estimating the amount of displacement during E1 is not straightforward in T3, for the reasons explained in the following. Should fault B (on which most of the displacement took place) have been a purely dip-slip fault, stratigraphic separation along the fault trace on the wall (SSAF; Figure 5h) would equal dip-slip displacement, because the T3 walls are perpendicular to the strike of fault B. Minimum estimates for dip-slip displacement during E1 would be possible to obtain by subtracting the stratigraphic separation along the fault trace on the wall (SSAF) of the base of U1 (1954 slip only) from the distance (along the fault trace on the wall) between the erosive top of U7b2 on the upthrown block, and the –depositional- top of U7b2 on the downthrown block. The respective measurements are shown in Figure 5h. Projection of the top of U7b2 to the fault is necessary on the NW wall, to avoid the complexity caused by the secondary fault T. Subtracting SSAF measurements for U1 from minimum SSAF measurements for the top of U7b2, we obtain ~75 cm of minimum SSAF to be attributed to E1 on the NW wall, and ~0 cm on the SE wall. These estimates do not reflect neither the true amount of dip-slip displacement though, nor its true difference from one wall to another. This is so, because fault B is oblique-slip, and because the pre-faulting ground surface (the top of U7b2) was horizontal in a direction parallel to the strike of the fault. The top of U7b2 on the downthrown block had a very strong average apparent dip to the NW, i.e. parallel to the strike of fault B. In specific, the elevation difference between the meeting points of the top of U7b2 (on the downthrown block) with the fault, was 0.9 m, at a distance of about 2.3 m only. A dip to the NW, combined with left-lateral horizontal displacement, results in stratigraphic separations of opposite sense compared to the sense of dip-slip displacement. An "*en fâce*" view of the fault plane is suitable to demonstrate this graphically (Figure 5i). In Figure 5i, we trace the top of U7b2 on the hangingwall block, before and after displacement event E1. For simplicity, Figure 5i shows only the strike-slip component of displacement (not the vertical displacement). Being a projection of the –inclined- fault plane to a vertical plane (striking parallel to the fault plane), rather than SSAF, Figure 5i shows the VSS that results from strike-slip displacement.

Considering that the erosive top of U7b2 on the upthrown fault block is at the same level on both walls, if no important change in the amount of E1 displacement occurred between the two walls (as it didn't in 1954), the much smaller minimum value for

the SSAF of the top of U7b2 that is measured on the SE wall (Figure 5h), suggests that there, the gradient of the pre-faulting ground surface (the top of U7b2) cannot have been the same as on the NW wall. Otherwise, there would be no such substantial difference in separation. Therefore, Figure 5i does not depict the real geometry of the top of U7b2 on the downthrown fault block. The two possible generic cases of alternative geometries that, for a given amount of strike-slip displacement (SS), can account for important differences in VSS (and SSAF) from one wall to another are shown in Figure 5j and k. In Figure 5j, strike-slip displacement produces VSSs that on both walls are of opposite sense compared to vertical displacement (not shown), but, "opposite-sense VSS" is larger on the SE wall. In Figure 5k, "opposite-sense" VSS on the SE wall, occurs at the same time as VSS adds up to vertical displacement on the NW wall. If we consider the scenario involving the gentler geometry (Figure 5j) to be more probable, the observed ~75 cm of minimum E1 SSAF of the top of U7b2 on the NW wall would then be a minimum value for the on-fault dip-slip displacement during E1. This value would be a minimum both because of erosion of U7b2 on the footwall block, and because of the "opposite sense" of SSAF produced by strike-slip displacement.

Event E2

Event E2 is clearly defined by U8 (T1 NW wall – Figure 3d), the largest wedge of "debris facies" colluvium in all three trenches. Unit 8 corresponds to the "lower debris element" in the classification of *Nelson* [1992]. It has a sharp contact with U9 and buries the very well developed soil horizon Bk2 (on U9), features in keeping with deposition from a scarp free face after faulting [e.g. *Swan et al.*, 1980; *Nelson*, 1992].

Unit 8 is a composite debris wedge. The upper part (U8a) consists of fine-pebble sized pieces of crushed bedrock (wBR) of the same facies as on the footwall block of fault B. Unit 8a has a sharp contact with the lower part of the wedge (U8b), which consists of larger pieces of wBR, mixed with carbonate deposits and fine-grained sediment. Given that no calcic soil development is observed on U7c or U8a right above U8b (NW wall), or on U7d, right above U9 (SE wall), the carbonate deposits and fine sediment in U8b are interpreted as reworked material from the part of the pre-faulting soil (U9/Bk2) that was exposed on the free face of the E2 scarp, as in the model of *McCalpin and Berry* [1996]. The composition of U8b, presumably resulted from "slumping" of the free face right after faulting [e.g. *Nelson*, 1992]. The fact that we do not recognize a relevant slumping scar on unit wBR, can be attributed to horizontal displacement by post-E2 events, which has translated the U8 feeder area to the SE of the NW wall of T1.

The triangular shape of U8a, i.e. its thickening towards fault B, suggests deposition of colluvium transported more or less perpendicular to the E2 scarp. The rather steep dip of the top of U8a is partially the result of forward tilt due to normal fault drag, as suggested by the geometry of the base of both U8a and U8b. In contrast, U8b was not thickening towards the fault, suggesting that it consists of debris transported parallel to the fault. That is, U8 lacks a regular triangular shape because of its composite nature, resulting from deposition of material derived from two different locations on the scarp.

On the SE wall of T1, U8 is absent. The event horizon of E2 is buried by U7d, a unit conspicuously richer in angular clasts of "healthy" bedrock, sourced from unit BR, not wBR. These clasts are also larger than those in the units above and below U7d. Unit 7d has a very sharp contact with the underlying U9, and locally, with the overlying U7c (Figure 10b). We interpret U7d as the debris element of scarp-derived colluvium. The locally very sharp U7d/U7c contact represents the abrupt transition between debris and wash facies of scarp-derived colluvium [*McCalpin and Berry*, 1996].

Unit 7d originated from a part of the E2 scarp that did not expose unit wBR at its free face, but only the fines of U9 and regolith from the healthier bedrock (BR) or, also a limited(?) exposure of the bedrock itself. The source area of U7d is not the footwall block exposed on the SE wall of T1 (where wBR does exist). Due to the sinistral horizontal displacement that post-E2 faulting has caused, the source area of U7d lies somewhere to the SE of the SE wall of T1. The fact that the wBR wedge between faults A and B tapers out towards the SE wall agrees with provenance of U7d from a scarp free face with little wBR or none at all. The fact that U7d does not exhibit thickening towards the fault zone (i.e. it does not have a typical wedge-like shape), suggests that the SE wall intersected a part of the wedge that was fed by debris facies colluvium transported predominantly parallel to the fault scarp. Such an interpretation complies with the analogy made by *Nelson* [1992] between colluvial wedges and coalesced alluvial fans (in "micrography").

On the SW wall of T3, E2 is evidenced by a small wBR-derived debris wedge above U9/Bk2 (U8 in Figure 5c and d), this time having a typical triangular shape. On the NW wall of T3, a debris unit similar to U8 or U7d was not discernible. Nevertheless, event E2 was indicated by a small fissure within U9, formed by fault B and a small antithetic fault, and by backtilting of U9 towards fault B. Backtilting was evidenced by thin beds of carbonate accumulations in Bk2 (U9) and the orientation of elongate/flat pebbles within U9. The entire scarp-derived colluvial wedge of E2 (debris and wash element together) in T3 extends up to the top of U7b2, as discussed earlier. The limits of the entire wedge associated to E2 in T1, will be discussed in the following.

More events between E1 and E2?

Very uncertain indications of an extra event between E1 and E2 ("event E2a") were found only on the SE wall of T1. A discontinuity that might possibly be a buried, minor synthetic fault was discernible about 1 m above the event horizon of E2 ("fault" W; Figure 3a). Also, a somewhat increased concentration of fine/medium pebble-sized bedrock clasts within a part of U7b between fault F and discontinuity E (a crack, or a fault hosting very small displacement) could correspond to debris facies of scarp-derived colluvium, but, more evidence are certainly required to support such an interpretation. The relevant part of U7b is marked with green question-mark in Figure 3a, because tracing a lithostratigraphic limit was not possible.

Another line of evidence that might be related to an "event E2a" is the geometry of paleochannel 2 (U5) in map view. Based on the occurrences of U5 in T1 and T2, paleochannel 2 trends roughly perpendicular to the ERZ and is deflected left-laterally along it (Figure 2 inset). This marked deflection suggests that a morphological anomaly existed along the ERZ before the establishment of the channel (i.e., before E1). Yet, this morphological anomaly need not necessarily be the result of a post-E2 / pre-E1 event of ground deformation. It can very well be a remanent feature related to event E2.

Given that we had four different wall exposures to look for evidence of "E2a", the available indications are too few and too weak to be conclusive. On the NW wall of T1, also E1 was not identifiable by any kind of evidence, but it was seen in the other trench walls. Within U7 in T3 and the NW wall of T1, no tectonic, stratigraphic or pedogenic evidence of "E2a" were found. We may hypothesize that even if an "event E2a" did take place, it was not associated with slip comparable to that of E2, E1 and 1954, otherwise we would have seen more evidence in its support.

.

Estimates of fault displacement during E2

If we accept that an "E2a" event is very unlikely, minimum estimates for the vertical separation (VS) of the ground surface that E2 produced can be obtained from the "net thickness" of the associated scarp-derived colluvial wedge, after corrections for near-fault "thickness amplification" caused by back-tilting [*Pantosti et al.*, 1996]. On the SE wall of T1, the colluvial wedge that deposited after E2 is the entire U7. Given the back-tilting observed at the top of U9 for a distance of about 4.6 m from the fault, extension of the T1 bottom was carried out to clarify the far-field geometry of the top of U9 (Figure 3c), and to be able to accurately project the "far-field" pre-E2 ground surface to the fault (dashed horizontal line in Figure 3c). Because E2 is not the last slip event, the back-tilting observed today is partly the result of younger events also. Thus, by correcting thickness for all the back-tilting recorded today, we somewhat underestimate the true net thickness of the wedge of E2. This is acceptable, because we can only derive a minimum estimate for VS anyway. Measuring maximum net thickness at the location where erosion by paleochannel 2 was the least, we obtain a minimum value of 2.30 m VS (Figure 3c). The net thickness of the entire E2 colluvial wedge on the SE wall of T3 (U8, U7b3 and U7b2 together - Figure 8), after correction for back-tilting of U9, is about 1.60 m.

The minimum VS estimates obtained in both T1 (2.30 m; SE wall) and T3 (160 cm; SE wall), are much higher than the largest discrete VS observed in 1954 (1 m in the area of T2). The top of U9 is found at the same level on both walls of T3 (away from the back-tilted area near the fault), i.e. it's apparent dip parallel to the fault strike is negligible and thus VS should approximates true vertical displacement well. In T1, in the back-tilted area near the fault, the apparent dip of the U9 top parallel to the fault strike is such that left-lateral strike-slip would result to VS larger than true vertical displacement. However, net thickness of the E2 wedge was measured with reference to the "far-field" geometry of the U9 top (away from the back-tilted area near the fault), where the fault-parallel dip component was practically zero. Thus, VS in T1 also should be close to true vertical displacement.

Based on the above, and under the consideration that an event "E2a" is very unlikely based on the data available, compared to the largest discrete vertical displacement observed in 1954 in the broader trench area (~1 m in T2), the vertical displacement during E2 was substantially larger (130% and 60% larger, in T1 and T3, resp.). Larger surface displacement at one locality only, is not a safe indication that E2 was a larger earthquake than E1 or 1954 [see *Biasi and Weldon*, 2006]. It does show though that slip (displacement), on this part of the ERZ at least, has been variable, i.e. that the comparable slip observed during the last two earthquakes (1954 and E1) is not characteristic [*sensu Schwartz and Coppersmith,* 1984] over longer timescales.

Dating of events of fault slip

Archaeological dating of event E1

Dating of event E1 was based on the archaeological dating of ceramic sherds. After wall cut-backs, weathering and progressive natural collapse of wall parts, we ended up with a total of more than 200 sample groups. Each group consisted of 1 to more than 20 sherds. Sample group locations are given in *Palyvos and Pavlopoulos*, [2008] and more detailed

descriptions of the recovered material are given by *Froussou* [in press].

All the chronological evidence from sherds in different stratigraphic units in T1 and T2 is summarized in Figure 10a, based on age ranges reported in Figure 9. The placement of sample S13 below U3 in Figure 10a is conventional, since U3 was not present on the trench wall S13 was found on (T2, NNW wall). From the topmost part of U3 upwards, stratigraphic units contained a mixture of ceramic sherds of different periods and different amount of wearing caused by transportation. Unit 4 and lower ones contained sherds thet belong exclusively to the Neolithic period and have generally been subjected to very little or little transportation.

The maximum (oldest) possible age of the youngest transported sherds in a unit, provides a *terminus post quem* (TPQ, or maximum-limiting age) for this unit and any event above it. Thus, the ages of the sherds in U6 and U5 provide a TPQ for event E1, placing it sometime after 4800 BC (6750 BP), possibly after 4500 BC (6450 BP); Figure 10a.

At the U4/1b contact in Trench 2 (NNW wall), many fragments of the same, large piece of closed vessel, were found concentrated at one location, buried by U1b (sample S13 in Figure 9a, location in Figure 4b). This indicates that the vessel piece broke apart at the findspot. The size of the reconstructed vessel piece, and the fact that the vessel walls were very thin ("eggshell"–like), suggest that the vessel piece was either transported (discarded) by a human or, that it was in any case subjected to very limited transportation by natural processes, before breaking at the findspot. I.e., the vessel piece has practically the same value as *in situ* archaeological features, and provides a minimum-limiting age (*terminus ante quem* – TAQ) for underlying stratigraphic units. The minimum (youngest) possible age of the reconstructed vessel piece (Figure 9b), provides a TAQ for U4, and thus also for event E1, which is placed before 2500 BC (4450 BP); Figure 10a.

Unit 4 (Figure 7a/b) is by far the richest in archaeological material (Figure 9c), and interpreted as a colluvium derived from human occupation horizons lying a short distance uphill of the trenches. That the archaeological material in U4 has been transported only for a very short distance is indicated by the abundance of this material, its local concentration (U4 was absent in T3), the sharp edges and angles of all sherds, the presence of large pottery fragments (e.g. Figure 9e), including a body fragment that was not broken to small flat pieces during transport but retained its round shape (Figure 9d), the abundance of pieces of charcoal (rare or absent in other units) and bone fragments, the dark gray color of the matrix (suggesting richness in material derived from burns) and the local presence of a blackish-gray horizon (below sub-unit 4a, discernible also in Figure 9c), which indicates very limited reworking of burn material.

Regarding the dating of E1, a critical issue is whether the potsherds in U4 were (a) derived from (or, mostly from) a pre-E1 deposit that was present on the scarp that E1 formed (i.e., U4 contains only, or mostly scarp-derived colluvium and all sherds are reworked), or, (b) produced (or, mostly produced) after E1 in the broader area of the trench during the deposition of U4 (i.e. U4 contains also, or mostly colluvium fed by deposits related to human activity during the deposition of U4 at an area very near the scarp of E1). Human activity in this case might also include the disposal of debris produced by a possible seismic destruction of the Neolithic settlement, caused by E1.

As far as hypothesis (a) above is concerned, U6, which predates E1, has a lithofacies identical to U4 (except for calcic soil development), and it was rich in sherds of the same age as those found in U4. Unit 6 was observed only on the SE wall of T1, as two small occurrences below U5, on both the downthrown and upthrown block. Fluvial erosion has affected the downthrown block (paleochannel 2, corresp. to U5; Figure 8), but, we still may say that a thick and laterally extensive U6 (capable of giving all the material in U4) probably did not exist. In such a case, we would also expect more of large and angular ceramic fragments within U5 (where such fragments were very rare). Little, if any U6 material was present on the free face that gave the debris wedge (which is located SE of the SE wall of T1 due to horizontal displacement in 1954), judging from the wedge's lack of substantial textural differentiation with the rest of U5a. But, the free face formed within a channel, so this does exclude the possibility that a thick deposit of U6 material did not exist just outside (SW of) the channel, i.e. very near the crest of the scarp. Unfortunately, erosional surfaces ES4 and 2 (Figure 8) truncate the pre-E1 stratigraphy at the upthrown block, thus it is unknown just how extensive U6 may have been there.

In T2, the erosion that produced erosional surfaces ES4, 2 and 1 (Figure 8) does not allow clarification of the above issue. However, the occurrence of U4 at the most distal part of the SSE wall is at such a distance from the fault zone that does not comply with a scarp-derived colluvial deposit. Furthermore, at this location U4 contained a characteristic facies assemblage that was observed also on the downthrown block in both T1 and T2 (sub-unit 4a, described in Figure 4). The above observations, together with the presence of ceramic fragments like the one in Figure 9d, which perhaps are not easy to reconcile with reworking (erosion and redeposition), suggest that hypothesis (b) is perhaps more likely than (a). If this is accepted, the fact that the sherds within U4 have been subjected to very little transportation, suggests that their minimum possible age can be used to derive a TAQ for E1, which is thus placed before 3800 BC (5750 BP).

Summarizing, E1 took place for sure between 6750 BP and 4450 BP, more likely between 6450 and 5750 BP. For use in earthquake catalogs, we conventionally

place it at 6100 ["conventional year", s*ensu Galli et al.,* 2008] +650 / -1650 BP.

Dating of event E2

Dating strategy / geological context of dated samples

To constrain the timing of event E2, dating of U9 or Bk2 (on U9) and of the first post-E2 colluvial sediment was desirable. Post-E2 colluvium (U7d, mainly) was dated first, in T1, before it's extension, and before the opening of T3 (which were done months later). After T3 was excavated, dating of potentially suitable Bk2 carbonate accumulations (not present in T1) was also attempted.

Unit 7d did not contain organic material, so dating was attempted with the optically stimulated luminescence (OSL) method. The sampled sediment was originally deposited in U9 on the upthrown block (presumably as an alluvial fan deposit), it was subsequently exposed on the scarp produced by event E2, and then reworked into scarp-derived colluvium that deposited in U7d. If the true age of U7d is to be derived, complete exposure to sunlight during colluvial transportation is a prerequisite. In respect of this prerequisite, distal facies of scarp-derived colluvium are considered best [*Forman et al.,* 1991, 2000]. In our case, because the initial length of T1 allowed for collection of samples only at relatively short distances from the paleo- fault scarp of E2, whether the condition of complete solar resetting is satisfied was not known *a priori*. The true transportation distances of the sampled scarp-derived colluvium are larger though than those that can be measured on the trench wall, (a) because T1 trends oblique to the fault, and (b) due to fault-parallel colluvial transport (see paleoseismological interpretation for U7d). Furthermore, detection of partial solar resetting is possible and, in any case, even a maximum-limiting age from partially reset sediment would be useful. Thus we proceeded with OSL dating of four samples (locations in Figure 3a).

Unit 9 did not contain organic material either and, OSL dating of sediment coming from horizons with pedogenic accumulations of carbonate (among other materials), i.e. the case of U9, is known to be problematic [e.g. *Forman et al.*, 2000]. After the excavation of T3, we explored the possibility of dating pedogenic carbonate coatings on cobbles found within U9 in the drainage pit at the distal part of T3 (Figure 5b). This carbonate is younger than the deposit in which it accumulated (U9). The question is, to which extent could some of this carbonate be younger than E2 as well.

Carbonate layers within Bk2 in T3 were clearly deformed by E2 close to the fault zone (NW wall), i.e. they pre-date E2. The morphological similarity between Bk2 in the area of these deformed layers and in the rest of T3, indicates lack of (or, lack of appreciable) "lateral weakening" of Bk2 [*McCalpin and Berry*, 1996] moving towards the fault. This is an indication that *most* of the soil formation that produced Bk2, took place before event E2 [*McCalpin and Berry*, 1996]. However, because of the lateral progradation of the colluvial wedge, burial of the pre-faulting soil occurs at progressively later times beneath increasingly distal parts of the wedge [*McCalpin and Berry*, 1996]. Thus, in the distal part of T3, Bk2 should include some carbonate that precipitated "soon after" E2. "Soon after" is by necessity qualitative. Pedogenic carbonate co-eval with Bk1 is not expected in Bk2 though, as suggested by the vertical distance between the lower limit of Bk1 and the upper limit of Bk2 in the distal part of T3 (Figure 10c). Such a possibility is even smaller at the stratigraphic level of sampled carbonate coatings, which come from cobbles and small boulders at a considerable depth (45-80 cm) below the upper limit of Bk2. The above considerations apply under the assumption that the major process responsible for the formation of Bk2 carbonate was precipitation by downward percolating soil solutions [e.g. *Bachman and Machette*, 1977].

The ^{14}C and U-series (TIMS) methods have been successfully applied to stone coatings [*Amundson et al.*, 1994; *Wang et al.*, 1996; *Sharp et al.,* 2003; *Pustovoytov et al.*, 2007a, b]. We used ^{14}C dating of pedogenic carbonate, which is based on the fact that pedogenic carbonate forms in carbon isotopic equilibrium with soil CO_2 [*Cerling*, 1984; *Cerling et al.*, 1989]. Theoretically, ^{14}C dating of pedogenic carbonate can be complicated by contributions of radiometrically dead carbon originating from detrital lithogenic carbonate [*Amundson et al.*, 1989] or, from decomposition of old fractions of soil organic matter [*Wang et al.*, 1994]. However, multiple datings of thin laminae of pedogenic carbonate coatings from Eurasian archaeological sites of known age have not indicated appreciable amounts of too old inorganic carbon fractions [*Pustovoytov et al.*, 2007a, b]. This encouraged us to apply radiocarbon dating of stone coatings in Bk2.

Luminescence (OSL) dating of Unit 7d (Trench 1)

Optically stimulated luminescence geochronology is based on the time-dependent dosimetric properties of silicate minerals, predominately quartz and feldspar [*Aitken*, 1998]. The sediment samples were analyzed at the Luminescence Dating Research Laboratory (Univ. of Illinois at Chicago) following the procedures described below.

Multiple-aliquot regeneration (MAR) [*Singhvi et al.*, 1982; *Jain et al.*, 2003] protocols were used to estimate the equivalent dose on fine-grained polymineral fraction from sediments (Table 1).

Laboratory solar resetting of natural luminescence was by an 8-hour exposure to 275 w GE Mercury Vapor Sunlamp, which is effective in evicting electrons from photosensitive traps [*Richardson*, 1994]. Luminescence measurements were completed on a Daybreak 1100 reader with light emitting diodes delivering infrared excitation (880 ± 80 nm) and blue light (470 ± 20 nm). The resultant blue emissions were measured with Schott BG-39 and Corning 7-59 filters in front of the photomultiplier tube.

To compensate for laboratory-induced sensitivity changes we used component specific normalization procedure [cf. *Jain et al.*, 2003]. A normalization dose (~82 Gy β) was applied to all discs prior to analysis and the ratio of secondary to initial luminescence response was used to derive a correction factor for sensitivity changes. The efficacy of the preheat treatment for the normalization dose was evaluated by comparing curve shape (trap distribution) between the natural and subsequent dose. A similar dose response was indicated by zero or low slope (<0.1) between the luminescence for initial and secondary dose, evaluated at one-second intervals. A preheat of 150º C for 1 hour yielded a luminescence distribution most similar to the natural emissions. Initially, the MAR procedure determined equivalent dose with infrared (IR) stimulation, and subsequently with blue light excitation. The integral for the first 30 seconds, in one-second intervals, of the glow down curves was used to calculate weighted mean equivalent dose (Table 1). This sequence of analysis (infrared followed by blue excitation) preferentially measures feldspar-sourced and then quartz emissions [cf. *Banerjee et al.*, 2001; *Roberts et al.*, 2001].

MAR protocols provide also necessary insight into partial solar resetting of the natural luminescence, which could lead to age overestimates. If the sediment is fully solar reset the natural shine down curve geometry, reflecting fast, medium and slow luminescence components [cf. *Singarayer and Bailey*, 2003] should parallel the response to laboratory radiation. In turn, the equivalent dose across the shine down curve should be uniform, with full solar resetting.

To render an optical age the environmental dose rate is needed, which is an estimate of sediment exposure to ionizing radiation from the decay of the U and Th series and ^{40}K, and cosmic sources during the burial period (Table 1). The U and Th content of sediment assuming secular equilibrium in the decay series and ^{40}K were determined by inductively coupled plasma-mass spectrometry (ICP-MS) analyzed by Activation Laboratory LTD, Ontario, Canada. A small cosmic ray component of 0.12 or 0.13 ± 0.02 mGy/yr, for the indicated depth of sediment, was included in the estimated dose rate [*Prescott and Hutton*, 1994]. A moisture content of 15 ± 5% was considered, which at two sigma errors covers the likely moisture content variation during the burial period.

All dating results are summarized in Table 1. In Figure 10d, the OSL dating results are depicted as reported in Table 1, with 1 sigma error ranges. Three of the samples were examined under both blue light and infrared excitation. The emissions from infrared and blue light excitation of these 3 samples, yielded ages that overlap at 1 sigma (Figure 10d) and, tests for anomalous fading for both components over 30 days yielded no diminution in signal. Thus, we conclude that the emissions associated with infrared and blue light excitation are thermally stable and time sensitive. I.e., the agreement between IR and BL age tests and confirms the general robustness of the OSL ages, i.e. that the obtained ages reflect burial time of the analysed sediment. Modest partial solar resetting (< 30% of the luminescence was inherited) was seen in the luminescence response of two out of three sediments analysed by IR excitation also (samples OSL4 and OSL2), and the equivalent dose was subsequently corrected.

To constrain the age of U7d and the timing of faulting, only the blue (BL) OSL ages are used because of the known signal stability and sensitivity to solar resetting [*Bulur et al.* 2000; *Wintle and Murray*, 2000]. If we are to have 95 % (instead of 67.5 %) probability for our interpretation, we need to compare dating results with 2 sigma error ranges (shown in Figure 10e). At 2 sigma confidence level, all ages overlap, thus are not statistically different. This evidence would suggest that the colluvium dated was deposited well within 1 to 2 standard deviations (1-3 ka). Consequently, OSL dating does not have the resolution to infer age trends within the colluvial unit 7d.

The weighted mean of all BL ages at 2 sigma (95 %) confidence level (17720 +- 4580 BP, plotted with solid line in Figure 10e), provides the most robust estimate for the average value of the burial age of the analyzed sediment samples, i.e. an average burial age for U7d. Unit 7d being above the event horizon of E2, the minimum possible value for average burial age (i.e. the minimum possible value for the weighted mean of all BL ages), provides a minimum-limiting age (*terminus ante quem*) of 13140 BP for event E2.

It is probable that the OSL average age obtained for U7d is a close age estimate of event E2, because: (a) the colluvial sediment within U7d expectedly started to deposit immediately after E2 took place (because it derives from the erosion of the respective fault scarp), (b) the debris element of scarp-derived colluvium (as U7d is), is supposed to accumulate relatively quickly [*e.g. Nelson, 1992*] and, (c) three out of four samples come from very near the base of U7d. As far as (b) is concerned, the sharp contrast between Bk2 and the carbonate-"free" U7d (Figure 10b), clearly suggests that U7d deposited faster than the sediment in U9 (assuming no change in soil-forming conditions other than the sedimentation rate).

Summarizing, the OSL results place event E2 at 95% probability before 13140 BP (at 67% probability, before 15430 BP). Accepting that the age of event E2 should be close to the age derived for U7d, the maximum possible age obtained for U7d (22300 BP, at 95% probability, 20010 BP at 67.5% probability), is a maximum-limiting age for E2 also. Based on the 1 sigma error range we conventionally assign E2 a preferred age of 17500 ("conventional year" *sensu* Galli et al., 2008) +- ~2500 BP for use in earthquake catalogs.

^{14}C dating of pedogenic carbonate coatings in Bk2

Pedogenic carbonate stone coatings in Bk2 (U9) at the distal part of T3 were randomly scattered over the surface of every single stone (cobble). Those sampled were detached from the stones on site, using a pocket knife as a lever. The thickest coating samples, from two different stones, were pretreated for ^{14}C (AMS) dating as described in *Pustovoytov et al.* [2007a, b]. Four sub-samples (C1-C4) of material from these two coatings were selected for dating. Samples C1 to C3 come from successive micro-layers of the same coating sample. C1 is the innermost layer, immediately above the stone, C2 the middle one and C3 the most exterior layer. Sample C4 was the innermost layer from another coating sample. Radiocarbon dating with the AMS method (Table 2) was carried out by the "Centro di Datazione e Diagnostica" of the Salento University.

The delta ^{13}C values of coating layers (Table 2) are typical for pedogenic carbonate [*Cerling*, 1984; *Cerling et al.*, 1989]; i.e., carbonate formed in isotopic equilibrium with soil CO_2 from soil solutions moving vertically downwards in the soil profile. The ages of C2 and C3 are in the correct stratigraphic order (middle and outer microlayer respectively). By contrast, the age for sample C1 (innermost microlayer) is younger than both the ages of C2 and C3. We hypothesize that this inversion in numerical ages might be due to: (a) the existence of active zones of secondary (pedogenic) carbonate precipitation at the coating-stone interface [*Brock and Buck*, 2005], which may have led to precipitation of new portions of carbonate in the space between the stone and the coating or/and, (b) re-crystallization of the innermost laminae of the coating. In hypothesis (a), the C1 and C4 ages can be treated the same way as those of C2 and C3, i.e. as maximum-limiting ages for E2 (subject only to the uncertainty stemming from the geological context of progressive burial of the pre-faulting ground surface and of Bk2 by post-E2 scarp-derived colluvium), but in hypothesis (b) they may underestimate E2's age. Some elements of the coating morphology seem to be in line with hypothesis (b): the inner coating surface was corroded in many places and locally covered by Mn-oxides, testifying to a change of the geochemical regime in the Bk horizon. Even so, at face value, the ^{14}C ages are still consistent with the weighted average of both 2 and 1-sigma optical ages of sediment in U7d (Figure 10e). One of the ^{14}C ages (C4) falls within the 1 sigma error range of the weighted average, and the other three (C1 to C3) are older, in agreement with the geological interpretation that the dated carbonate accumulated before, or "soon after" the beginning of the colluvial depositional event that produced U7d in response to scarp formation by E2. .

Considering the uncertainty about the exact significance of the youngest coating ages, we will avoid using them to further refine the E2 age estimate from optical ages. The two oldest coating ages (C2, C3) tell us that Bk2 probably started forming before ca. 24 ka BP, and in all likelihood at least 2000 years earlier than that, considering that the C2 age –now uncalibratable- will expectedly become substantially older if calibrated in the future. Based on the context of tectonic burial of soils by successive activations of the ERZ, the above minimum-limiting age for the initiation of Bk2 formation is a possible minimum-limiting age for the next previous (major) event of faulting (E3).

Constraints on recurrence intervals and slip rate

The elapsed time between E1 and the 1954 earthquake is ca. 6754-4454 yr, i.e. minimum 4454 yr. Based on a minimum age of 13140 or 15430 BP for E2 and a maximum age of 6750 BP for E1, we obtain 6390 or 8680 yr minimum elapsed time between E2 and E1. If we were to allow even for the possibility of an extra event ("E2a") between E1 and E2, using the smallest of the above minimum values (6390 yr) we would obtain a most conservative average recurrence interval estimate of 3195 yr. Based on all the above, the most recent past activations of the ERZ (excluding events of ground cracking like E1a), have an average recurrence interval of at least 3195 yr. This result is in general agreement with the slow deformation rates in broader Thessaly, and millennial-scale earthquake recurrence periods proposed from previous paleoseismological results in NW Thessaly. Namely, those of *Caputo and Helly* [2005], which place the last event of the Rodia fault (R in Figure 1b) at about 2-3 ka BP, and of *Caputo et al.* [2006], who propose recurrence intervals of 2-4 kyr (or 1.5-3 kyr, in an alternative interpretation involving smaller-magnitude earthquakes) at the Tyrnavos fault (T in Figure 1b).

Whether ruptures at the ERZ necessarily accompanied *every* activation of the broader Domokos fault zone (DFZ), is a critical issue, given the complexity and sporadic nature of the 1954 ruptures. The fact that the ERZ was the longest of all the 1954 rupture zones along the DFZ, as well the results in our trenches, which identify two previous 1954-like

ruptures on the ERZ (E1 and E2), make such a hypothesis seem plausible. Yet, a definitive answer should best be given only after paleoseismological investigations are carried out also at other rupture zones along the DFZ.

Estimation of average slip rate of the ERZ requires measurements of cumulative displacement (slip) of dated stratigraphic markers. Displacement is estimated here from cumulative net vertical displacement and the pitch of the slip vector (striae on fault planes), using trigonometric relationships. In the following, we use the pitch of the striae at the deeper part of the trenches. If the pitch of the mean slip vector in each trench is used instead, slightly smaller values are obtained.

Because of the oblique-slip character of the fault, we can measure directly only cumulative vertical stratigraphic separation (VSS), which approximates true cumulative vertical displacement only in contacts that have a small fault-parallel dip component. The only such contact that appears on both the downthrown and upthrown blocks and has experienced more slip than just that of 1954, is the base of U5 (paleochannel 2) on the SE wall of T1 (133 cm cumulative VSS, translating to about 213 cm of net slip). Using the maximum and minimum possible ages of E1 (after which the measured VSS accumulated), we obtain slip rates in the range 0.32-0.48 mm/yr. These values are an overestimate of average slip rate (if average slip rate is assumed constant over time), because the last displacement occurred in 1954, i.e., very recently. On the other hand, they do not include distributed deformation away from the fault.

For larger time spans, encompassing more events (i.e., also E2), only minimum estimates of cumulative VSS can be obtained, due to erosion on the upthrown block (ES1, ES2 and ES4 in Figure 8). As explained in the discussion of E2, VSS measured based on the far-field geometry of the top of U9, should approximate vertical displacement. Assuming that U9 existed on the upthrown block, as seems to be suggested by the composition of U8b, the vertical distance between the top of U9 on the downthrown block and the top of the bedrock on the upthrown block provides a minimum-limiting estimate for cumulative VSS since E2. The most conservative measurement is 286 cm, measuring immediately to the SW of fault B (Figure 3c). If we measure farther away on the upthrown block, to account for distributed deformation away from faults A and B, we get 403 cm instead. Distributed deformation is rather probable, considering that the erosional surface ES6 was in all likelihood horizontal or sub-horizontal originally, as evidenced in T3 and the WSW part of T2's SSE wall (Figure 8). Considering an age between 20300 and 15430 BP for E2, for 286 or 403 cm minimum VSS, which translate to 459 or 646 cm of minimum net slip (respectively), we obtain minimum slip rates of 0.23-0.30 or 0.32-0.42 mm/yr. In T3, the respective minimum VSSs (most conservative, across fault B only, and, probable, across the whole fault zone from fault A to B) are 105 and 276 cm, measured from the projection of the (inclined) top of U9 towards the upthrown block. They translate to 146 and 384 cm of minimum net slip, and a minimum slip rate of 0.07 to 0.25 mm/yr.

Summarizing, the slip rate of the ERZ at the trench site is of the order of 0.3-0.5 mm/yr (based on T1, where the largest cumulative displacement is observed) or, somewhat higher (but, expectedly below 1 mm/yr). This estimate is a minimum for the slip rate of the DFZ, because (a) slip rates estimated near the surface underestimate the slip rate at depth and, (b) the DFZ is complex and slip may be distributed to more faults at the surface than just the ERZ. These factors do not allow for a confident interpretation of the dramatic difference between our slip rate estimates at the ERZ and the 4 mm/yr slip rate that *Papadimitriou and Karakostas* [2003] propose for the entire DFZ [see *Caputo,* 2005 for objections, and *Papadimitriou and Karakostas*, 2005, for reply].

Conclusions

Observations on faulted colluvial and alluvial deposits exposed in three closely spaced trenches across the Ekkara rupture zone (ERZ, belonging to the Domokos Fault zone - DFZ) indicate that the 1954 co-seismic ground ruptures along the ERZ were tectonic, as proposed by previous researchers based on surface geological evidence only. Tectonic slip is verified by well-developed striae, which evidence a slip vector that does not comply with superficial ruptures of gravitational origin (due e.g. to settling of Holocene deposits abutting bedrock), and is instead in very good agreement with the direction of active extension in the broader area of Thessaly. The ERZ kinematics is oblique-normal, with an important left-lateral strike-slip (horizontal) component of displacement.

The paleoseismological interpretation of stratigraphic, soil-stratigraphic and tectonic evidence in the trenches reveals two prehistoric episodes of tectonic slip comparable to that of 1954 (episodes E1 and E2) on the ERZ since about 24000 BP. This indicates that paleoseismological investigations on sporadic rupture zones like the ERZ are justified.

Based on archaeological dating of transported ceramic sherds, event E1 occurred between 4800 and 2500 B.C. (6750 and 4450 BP), more likely between 4500 and 3800 B.C. (6450 and 5750 BP). For use in earthquake catalogs, we conventionally place it in 6100 +650 / -1650 BP. Event E1 was followed soon after by an episode of ground cracking along the ERZ, associated with zero or negligible slip (event E1a). Event E1a may correspond to an E1 aftershock on the DFZ or, sympathetic slip in response to activation of nearby fault zones, possibly triggered by E1 on the DFZ. Such a cracking event has not been reported after the 1954 earthquake.

Event E2 was in all probability associated with larger displacement than both younger events (E1 and 1954). This suggests that the comparable slip observed during the last two earthquakes (1954 and E1) at the trench location, is not characteristic over longer timescales. Larger slip at one location only does not necessarily suggest though that E2 corresponded to a stronger earthquake; observations at other locations along the DFZ are necessary if such a conclusion is to be drawn.

Optical (luminescence) dating of colluvial sediments places E2 ca. 13100-24000 BP, more likely at about 17500 +- ~2500 BP (preferred age). Radiocarbon ages of pedogenic carbonate (stone coatings) are consistent with the optical dating results and support the obtained age for E2 (albeit without allowing for further refinement), whereas they provide a likely constraint on the timing of the next oldest – major- event of faulting. Based on soil-stratigraphic considerations subject to verification by further studies, this event (E3) took place before 24000 BP.

The recurrence interval of recent ground ruptures similar to those of 1954 at Ekkara is estimated to be larger than 3195 yr, in a most conservative interpretation that allows for an extra event between E1 and E2 (for which no real evidence was found though). This result is in agreement with the millennial-scale earthquake recurrence periods proposed from previous paleoseismological studies elsewhere in Thessaly.

Given the complexity and sporadic nature of the 1954 ruptures along the DFZ, paleoseismological data from the ERZ only are insufficient to ascertain that ruptures with metre-scale displacement on the ERZ accompanied *each* past activation of the DFZ. The ERZ did host the most extensive of all 1954 surface faulting, and has ruptured repeatedly during the last 20000 yrs but, whether the paleoseismic record of the ERZ represents fully the paleoseismic record of the DFZ need better be clarified by further paleoseismological investigations, on *other* rupture zones along the DFZ.

Estimated slip rate of the ERZ is 0.3-0.5 mm/yr or somewhat higher (expectedly, not higher than 1 mm/yr). Slip rate estimates for the ERZ should not be generalized to the entire DFZ though, because, the complexity of the 1954 ground ruptures and of the geomorphic signature of the DFZ suggest that co-seismic deformation in the past may have been distributed to more than one rupture zones at the surface. Slip rate estimates for the ERZ, may thus underestimate the slip rate of the Domokos seismic fault zone.

Acknowledgements

This work was carried out in the frame of General Secretariat of Research & Technology project 04EP47 (re-patriation fellowship to N.P.) co-funded from the European Social Fund (75%), and the Hellenic State (25%, with 10% indirect funding from the private sector [Terra Ltd, Athens]). We warmly thank A. Marnieros for Terra's support in different parts of the project, the Director of the 14th EPCA, M.-E. Papakonstantinou for excavation permits and for assigning to E.F. the study of the ceramic material in the trenches, the president of the community of Ekkara S. Gournas and his family for their multi-faceted support, S.V. Gournas for permission to excavate in his field, H. Kaltsoulas for patient backhoe operation, the people of Ekkara and Velessiotes, who were always willing to provide any information they could on the 1954 ruptures, G. Quarta and L. Calcagnile (CEDAD) for excellent ^{14}C dating services, D. Pantosti for discussions at an early stage of the study, R. Paepe for discussion on the possible age of the deepest paleosoil, S. Pavlides, A. Chatzipetros, G. Syrides, K. Vouvalides and A. Ganas, and their students that visited the trench site and discussed with us in front of the trench walls, and two anonymous reviewers and the JGR editors for constructive and helpful suggestions of improvements of the original manuscript.

References

Ambraseys N.N., Jackson J.A., 1990. Seismicity and associated strain of central Greece between 1890 and 1988. Geophysical Journal International, 101, 663-708.

Amundson, R., Chadwick, O., Sowers, J. and Doner, H. 1989. The stable isotope chemistry of pedogenic carbonates at Kyle Canyon, Nevada. Soil Science Society of America Journal 53, 201–10.

Amundson, R., Wang, Y., Chadwick, O., Trumbore, S., McFadden, L., McDonald, E., Wells, S. and DeNiro, M. 1994. Factors and processes governing the ^{14}C content of carbonate in desert soils. Earth and Planetary Science Letters 125, 385–405.

Bachman, G. O., Machette, M. N., 1977. Calcic soils and calcretes in the southwestern United States. USGS Open-file report 77-794, 168 pp.

Banerjee, D., Murray, A.S., Botter-Jensen, L. and Lang, A., 2001. Equivalent dose estimation using a single aliquot of polymineral fine grains. Radiation Measurements, 33(1), 73-94.

Biasi, G.P., Weldon, R.J., 2006. Estimating surface rupture length and magnitude of paleoearthquakes from point measurements of rupture displacement. Bull. Seism. Soc. Am. 96, 1612–1623.

Birkeland, P. 1999. Soils and Geomorphology. Oxford University Press, New York.

Bonilla, M. G., Lienkaemper, I. J., 1990. Visibility of fault strands in exploratory trenches and timing of rupture events. Geology 18, 153–156.

Brock, A.L., Buck, B.J., 2005. A new formation process for calcic pendants from Pahranagat

Valley, Nevada, USA, and implication for dating Quaternary landforms. Quaternary Research, 63, 359-367.

Bronk Ramsey, C. 2001. Development of the radiocarbon program OxCal. Radiocarbon 43, 355–63.

Bulur, E., Bøtter-Jensen, L., and Murray, A. S. (2000) Optically stimulated luminescence from quartz using linear modulation technique, *Radiation Measurements*, v.32, no.5-6, pp.407-411.

Caputo, R., 2005, Comment on "Episodic occurrence of strong (Mw 6.2) earthquakes in Thessalia area (central Greece)" by E.E. Papadimitriou and V.G. Karakostas, Earth and Planetary Science Letters, 231 (3-4), pp. 347-352.

Caputo, R., 1995, Inference of a seismic gap from geological data: Thessaly (Central Greece) as a case study. Annali di Geofisica, XXXVIII (1), 1-18

Caputo, R., Helly, B., Pavlides, S., Papadopoulos, G., 2006. Archaeo- and paleoseismological investigations in Northern Thessaly (Greece): Insights for the seismic potential of the region. Natural Hazards 39, 195-212.

Caputo, R., Helly, B., 2005. The Holocene activity of the Rodia fault, Central Geece. Journal of Geodynamics 40, 153-169.

Caputo, R., Pavlides, S., 1993. Late Cenozoic geodynamic evolution of Thessaly and surroundings (central-northern Greece). Tectonophysics 223, 339-362.

Cerling, T. 1984. The stable isotopic composition of soil carbonate and its relationship to climate. Earth and Planetary Science Letters 71, 229–40.

Cerling, T., Quade, J., Wang, Y. and Bowman, J.R. 1989. Carbon isotopes in soils and paleosoils as ecology and paleoecology indicators. Nature 341, 138–39.

Chadwick, O., Sowers, J., Amundson, R. 1989. Morphology of calcite crystals in clast coatings from four soils in the Mojave Desert region. Soil science sosciety of America journal. 52. 211-219

DePolo, C., Clark, D., Slemmons, B., Ramelli, A., 1991. Historical surface faulting in the basin and range province, western north America: implications for fault segmentation. Journal of Structural Geology, 13 (2), 123-136.

Forman S. L., Pierson, J., Lepper, K., 2000. Luminescence Geochronology. pp. 157-176 In: Noller, J.S., Sowers, J.M., and Lettis, W.R. (Eds.), 2000, Quaternary Geochronology - Methods and Applications. American Geophysical Union, AGU Reference Shelf, 4, Washington, D.C.. 582 pp.

Forman, S.L., Nelson, A.R., McCalpin, J.P., 1991. Thermoluminescence dating of fault-scarp-derived colluvium – deciphering the timing of paleoearthquakes on the Weber segment of the Wasatch fault zone, north central Utah. Journal of Geophysical Research 96 (B1), 595-605.

Froussou, E., A new, unknown site with long-lasting human occupation at Ekkara in Fthiotis, Proceedings of the 3rd Archaeological meeting of Thessaly and Central Greece (AETHSE, 12-15th March 2009), in press.

Galli, P., Galadini, F., Pantosti, D., 2008. Twenty years of paleoseismology in Italy. Earth-Science Reviews 88, 89-117. doi:10.1016/j.earscirev.2008.01.001

Jain, M., Botter-Jensen, L., Singhvi, A.K., 2003. Dose evaluation using multiple-aquilot quartz OSL: test of methods and a new protocol for improved accuracy and precision. Radiation Measurements 37, 67-80.

McCalpin, J.P., 1996a. Field techniques in paleoseismology. In: McCalpin, J.P. (Ed.), Paleoseismology. Academic Press, pp. 33-84.

McCalpin, J.P., 1996b. Paleoseismology in extensional tectonic environments. In: McCalpin, J.P. (Ed.), Paleoseismology. Academic Press, pp. 85–146.

McCalpin, J.,P., Berry, M.E., 1996. Soil catenas to estimate ages of movements on normal fault scarps, with an example from the Wasatch fault zone, Utah, USA. Catena (27), 265-286.

McCalpin, J.P., Nelson, A.R., 1996. Introduction to Paleoseismology. In: McCalpin, J.P. (Ed.), Paleoseismology. Academic Press, pp. 1-32.

Nelson, A. R., 1992. Lithofacies analysis of colluvial sediments – an aid in interpreting the recent history of quaternary normal faults in the Basin and Range province, Western Unites States. Journal of Sedimentary Petrology 62 (4), 607-621.

Palyvos, N., Pavlopoulos, K., 2008. Acquisition of data for seismic hazard assessments, with paleoseismological and geomorphological methods. General Secretariat of Research and Technology, ENTER project no. 47 (04EP47), Final Report & Deliverables (in Greek). *(open access to all material at: http://www.hua.gr/geografias/kpavlop/programmata/2008_04EP47/Main.html) [requires the Mozilla Firefox web browser]*

Pantosti, D., D'Addezio, G., Cinti, F.R., 1996. Paleoseismicity of the Ovindoli-Pezza fault, central Apennines, Italy: A history including a large, previously unrecorded earthquake in the Middle Ages (860-1300 A.D.). Journal of Geophysical Research 101(B3), 5937-5959.

Pantosti, D., Schwartz, D. P., Valensise, G., 1993. Paleoseismology along the 1980 surface rupture of the Irpinia fault; implications for earthquake recurrence in the southern Apennines, Italy. Journal of Geophysical Research 98, 6561-6577.

Papadimitriou, E.E., Karakostas, V.G., 2005. Occurrence patterns of strong earthquakes in Thessalia area (Greece) determined by the stress evolutionary model. Earth and Planetary Science Letters 235, 766-770.

Papadimitriou, E.E., Karakostas, V.G., 2003. Episodic occurrence of strong (Mw ≥ 6.2) earthquakes in Thessalia area (central Greece). Earth and Planetary Science Letters 215 (3-4), 395-409.

Papadopoulos, G.A., 1992. Rupture zones of strong earthquakes in the Thessalia region, Central Greece, XXIII General Assembly Europ.

Seismol. Commis. Prague, September 1992, Proceedings, vol. 2, 1992, pp. 337–340.

Papastamatiou, D., Mouyiaris, N., 1986a. The Sofades earthquake of April 30, 1954 – Field observations of Giannis Papastamatiou. Geological and Geophysical Studies, sp. volume, 341-362.

Papastamatiou, D., Mouyiaris, N., 1986b. The earthquake of April 30, 1954, in Sophades (Central Greece). J. R. Astr. Soc. 87, 885-895.

Papazachos, B.C., Papazachou, C., 2002. The Earthquakes of Greece. Ziti Publications, Thessaloniki, 317 pp.

Papazachos, B.C. , E.E. Papadimitriou, A.A. Kiratzi, C.B. Papazachos, E.K. Louvari, Fault plane solutions in the Aegean Sea and the surrounding area and their tectonic implications, Boll. Geof. Teor. Appl. 39 (1998) 199-218.

Pavlides S., 1993. Active faulting in multi-fractured seismogenic areas: examples from Greece. Z. Geomorph. N.F., 94, 57-72.

Prescott, J. R., Hutton, J. T., 1994. Cosmic ray contributions to dose rates for luminescence and ESR dating: large depths and long-term time variations. Radiation Measurements 23, 497-500.

Pustovoytov, K., Schmidt, K., Taubald, H., 2007a. Evidence for Holocene environmental changes in the northern Fertile Crescent provided by pedogenic carbonate coatings. Quaternary Research 67, 315-327

Pustovoytov, K., Schmidt, K., Parzinger, H., 2007b. Radiocarbon dating of thin pedogenic carbonate laminae from Holocene archaeological sites. The Holocene 17 (6), 835-843.

Pustovoytov, K. 2002. Pedogenic carbonate cutans on clasts in soils as a record of history of grassland ecosystems. Palaeogeography, Palaeoclimatology, Palaeoecology. 177. 199-214.

Reimer, P.J., Baillie, M.G.L., Bard, E., Bayliss, A., Beck, J.W., Bertrand, C.J.H., Blackwell, P.G., Buck, C.E., Burr, G.S., Cutler, K.B., Damon, P.E., Edwards, R.L., Fairbanks, R.G., Friedrich, M., Guilderson, T.P., Hogg, A.G., Hughen, K.A., Kromer, B.,McCormac, G., Manning, S., Ramsey, C.B., Reimer, R.W., Remmele, S., Southon, J.R., Stuiver, M., Talamo, S., Taylor, F.W., van der Plicht, J., Weyhenmeyer, C.E., 2004. IntCal04 terrestrial radiocarbon age calibration, 0–26 cal kyr BP. Radiocarbon 46(3), 1029–1058.

Richardson, C.A., 1994. Effects of Bleaching On the Sensitivity to Dose of the Infrared-Stimulated Luminescence of Potassium-Rich Feldspars From Ynyslas, Wales. Radiation Measurements, 23(2-3), 587-591.

Roberts, H.M., Wintle, A.G., Maher, B.A. and Hu, M.Y., 2001. Holocene sediment-accumulation rates in the western Loess Plateau, China, and a 2500-year record of agricultural activity, revealed by OSL dating. Holocene, 11(4). 477-483.

Schwartz, D., and Coppersmith, K. (1984), Fault Behavior and Characteristic Earthquakes: Examples From the Wasatch and San Andreas Fault Zones, J. Geophys. Res., 89(B7), 5681-5698.

Sharp, W.D., Ludwig, K.R., Chadwick, O.A., Amundson, R., Glaser, L.L., 2003. Dating fluvial terraces by 230Th/U on pedogenic carbonate, Wind River Basin, Wyoming. Quaternary Research 59, 139–150.

Singarayer, J.S. and Bailey, R.M., 2003. Further investigations of the quartz optically stimulated luminescence components using linear modulation. Radiation Measurements, 37(4-5), 451-458.

Singhvi, A.K., Sharma, Y.P. and Agrawal, D.P., 1982. Thermoluminescence dating of dune sands in Rajasthan, India. Nature, 295: 313-315.

Swan, F.H., Schwartz, D.P., Cluff, L.S., 1980. Recurrence of moderate to large magnitude earthquakes produced by surface faulting on the Wasatch fault zone, Utah. Bulletin of the Seismological Society of America 70(5), 1431-1462.

Wang, Y., McDonald, E., Amundson, R., McFadden, L., Chadwick, O. 1996. An isotopic study of soils in chronological sequences of alluvial deposits, Providence Mountains, California. Geological Society of America Bulletin. 108. 379-391

Wang, Y., Amundson, R., Trumbore, S., 1994. A model for soil $^{14}CO_2$ and its implications for using ^{14}C to date pedogenic carbonate. Geochimica et Cosmochimica Acta 58, 393-399.

Weldon, R. J., J. McCalpin, and T. K. Rockwell (1996). Paleoseismology of strike-slip tectonic environments. In: McCalpin, J.P. (Ed.), Paleoseismology. Academic Press, pp. 271–329.

West, M.W., 1993. Extensional reactivation of thrust faults accompanied by coseismic surface rupture, southwestern Wyoming and north-central Utah. Geol. Soc. Am. Bull. 105, 1137-1150.

Wintle, A. G., and Murray, A. S. (2000) Quartz OSL: effects of thermal treatment and their relevance to laboratory dating procedures, *Radiation Measurements*, v.32, no.5-6, p.387-400.

Valkaniotis, S., 2005. Study of the active faults of Western Thessaly. MSc Thesis, Dept. of Geology, University of Thessaloniki, 118 pp.

Yeats, R.S., Sieh, K., Allen, C.R., 1997. The Geology of Earthquakes. Oxford University Press, New York. 568 pp.

Tables & Figures

Table 1. Results of Optically Stimulated Luminescence dating of sediment sampled from the base of unit 7d (colluvium originating from fine-dominated alluvial fan deposits). All errors are at one sigma.

Field Number and depth (m)	Laboratory Number[a]	Equivalent dose (Grays)	U (ppm)[b]	Th (ppm)[b]	K_20 (%)[b]	a value[c]	H_20 (%)	cosmic (mGrays/yr)[d]	Dose Rate (mGrays/yr)	IRSL age (yr)
OSL1 (4.40)	UIC2092BL	36.10 ± 1.04	0.7 ± 0.1	3.7 ± 0.1	1.44 ± 0.01	0.05 ± 0.01	15 ± 5	0.12 ± 0.01	1.94 ± 0.10	18,560 ± 1540
OSL2 (4.23)	UIC2094BL	28.60 ± 3.53	0.4 ± 0.1	2.0 ± 0.1	1.04 ± 0.01	0.04 ± 0.01	15 ± 5	0.12 ± 0.01	1.32 ± 0.11	21,690 ± 3080
OSL2 (4.23)	UIC2094IR	31.76 ± 1.08[e]	0.4 ± 0.1	2.0 ± 0.1	1.04 ± 0.01	0.06 ± 0.01	15 ± 5	0.12 ± 0.01	1.34 ± 0.08	23,620 ± 2090
OSL3 (4.09)	UIC2091BL	30.51 ± 0.63	0.7 ± 0.1	3.7 ± 0.1	1.39 ± 0.01	0.06 ± 0.01	15 ± 5	0.12 ± 0.01	1.92 ± 0.10	15,915 ± 1300
OSL3 (4.09)	UIC2091IR	33.65 ± 0.38	0.7 ± 0.1	3.7 ± 0.1	1.39 ± 0.01	0.08 ± 0.01	15 ± 5	0.12 ± 0.01	1.97 ± 0.10	17,040 ± 1350
OSL4 (3.63)	UIC2093BL	31.77 ± 0.72[e]	0.5 ± 0.1	2.8 ± 0.1	1.34 ± 0.02	0.06 ± 0.01	15 ± 5	0.13 ± 0.01	1.72 ± 0.10	18,455 ± 1540
OSL4 (3.63)	UIC2093IR	32.46 ± 0.30	0.5 ± 0.1	2.8 ± 0.1	1.34 ± 0.02	0.09 ± 0.01	15 ± 5	0.13 ± 0.01	1.80 ± 0.10	18,050 ± 1470

Table 2. Results of radiocarbon dating of carbonate coatings on stones retrieved from unit 9 (Bk horizon of paleosoil 2) in Trench 3. Samples C1-C3 come from successive micro-layers in the thickest piece of coating retrieved. Sample C4 came from a coating on a different stone. Dating conducted by CEDAD (Centro di Datazione e Diagnostica, Dipartimento di Ingegneria dell'Innovazione, Università del Salento, Italia). Calibration was done with Oxcal [*Bronk Ramsey,* 2001]), using the "Intcal04" calibration curve [*Reimer et al.*, 2004].

Sample code	**Lab. Number**	**$^{13}C/^{12}C$ ratio (‰)**	**Conventional R/C age ($^{13}C/^{12}C$ corr.)**	**Calibrated R/C age [2 sigma (95.4%) probability]**
C1	LTL3154A	[not reported by laboratory]	17894 ± 110	21129 ± 435
C2	LTL3155A	-7.5 ± 0.2	24130 ± 130	outside Intcal04 calibration range
C3	LTL3156A	-7.5 ± 0.5	20181 ± 100	24167 ± 281
C4	LTL3157A	-7.5 ± 0.4	14560 ± 60	17515 ± 415

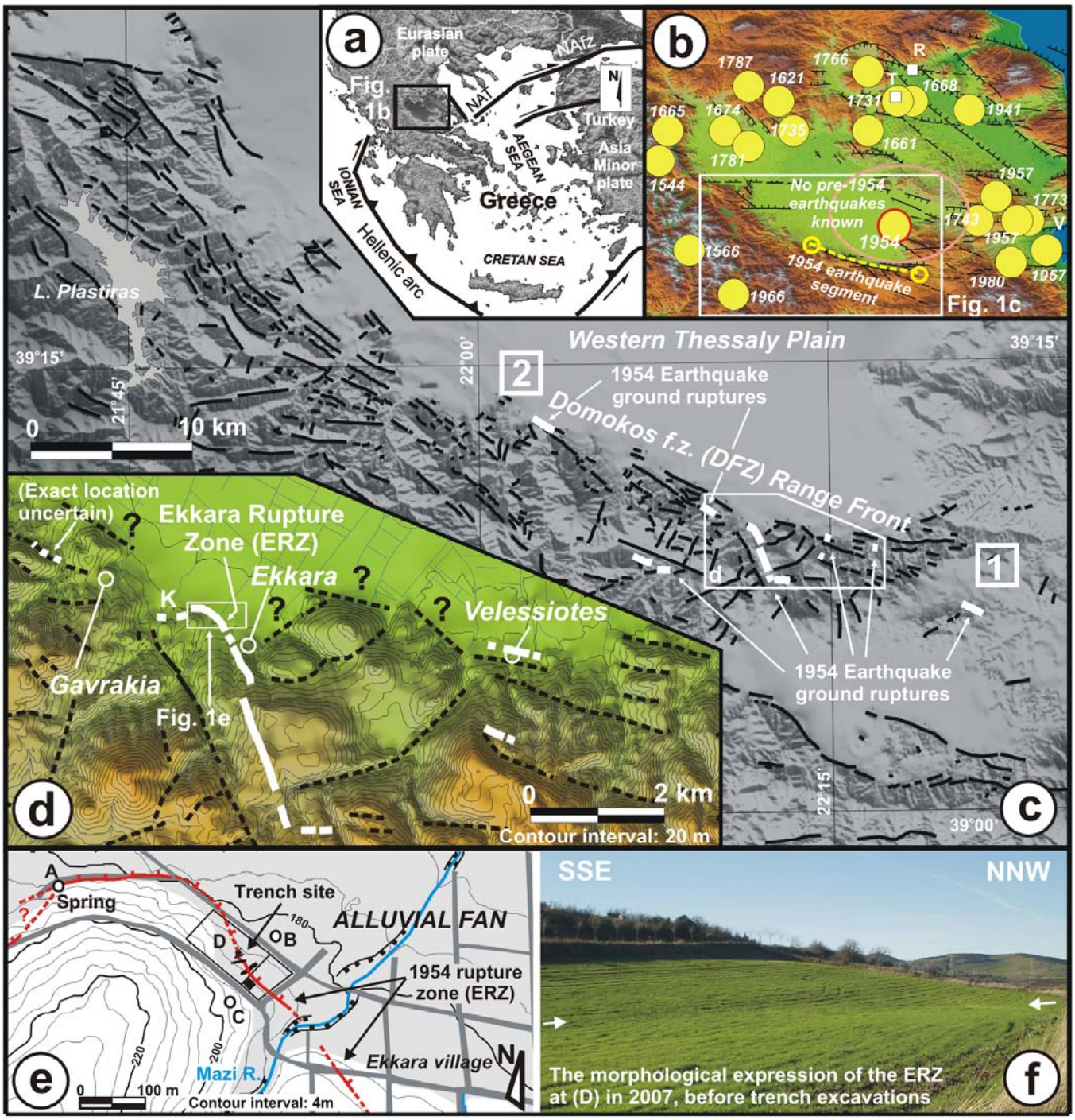

Figure 1. a: Location map. **b:** Neotectonic fault zones [from *Caputo and Pavlides, 1993*] and approximate locations of historical earthquake epicentres in Thessaly [from *Papazachos and Papazachou*, 2002]. **c:** Morphotectonic discontinuities of undifferentiated origin along the southern boundary of the Western Thessaly Plain [from *Palyvos and Pavlopoulos*, 2008], and the sporadic ruptures that accompanied the 1954 earthquake [from *Papastamatiou and Mouyiaris*, 1986; *Ambraseys and Jackson*, 1990]. **d:** the Ekkara rupture zone [from *Papastamatiou and Mouyiaris*, 1986]. Question-marks indicate morphotectonic discontinuities that are mostly interpretative. **e:** Location of trench site and re-mapped trace of the 1954 rupture. **f:**.View of the 1954 scarp after 53 years of degradation (natural and due to cultivation) at location D, in 2007. Trench 1 was excavated in the area at the left hand side of the photograph.

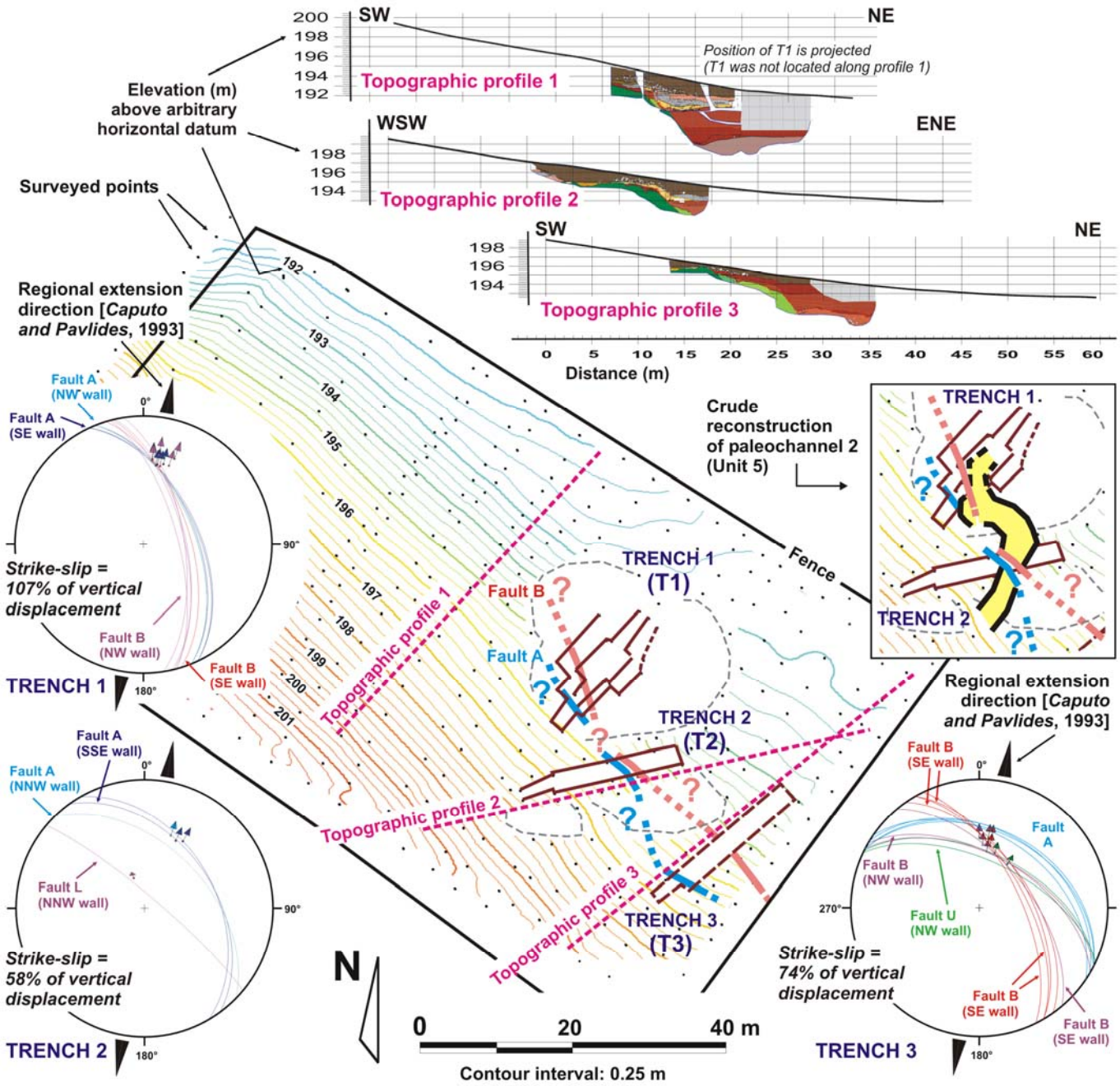

Figure 2. Detailed topographic map and profiles of trench site (from field survey with total station). Stereoplots (equal area, lower hemisphere projection) show measurements of fault planes and striae. Fault labels (A, B) as in the trench logs. Inset shows a crude reconstruction of paleochannel 2 (Unit 5), which exhibits a marked left-lateral deflection along the ERZ. Left-lateral horizontal displacement of paleochannel 2 is much smaller.

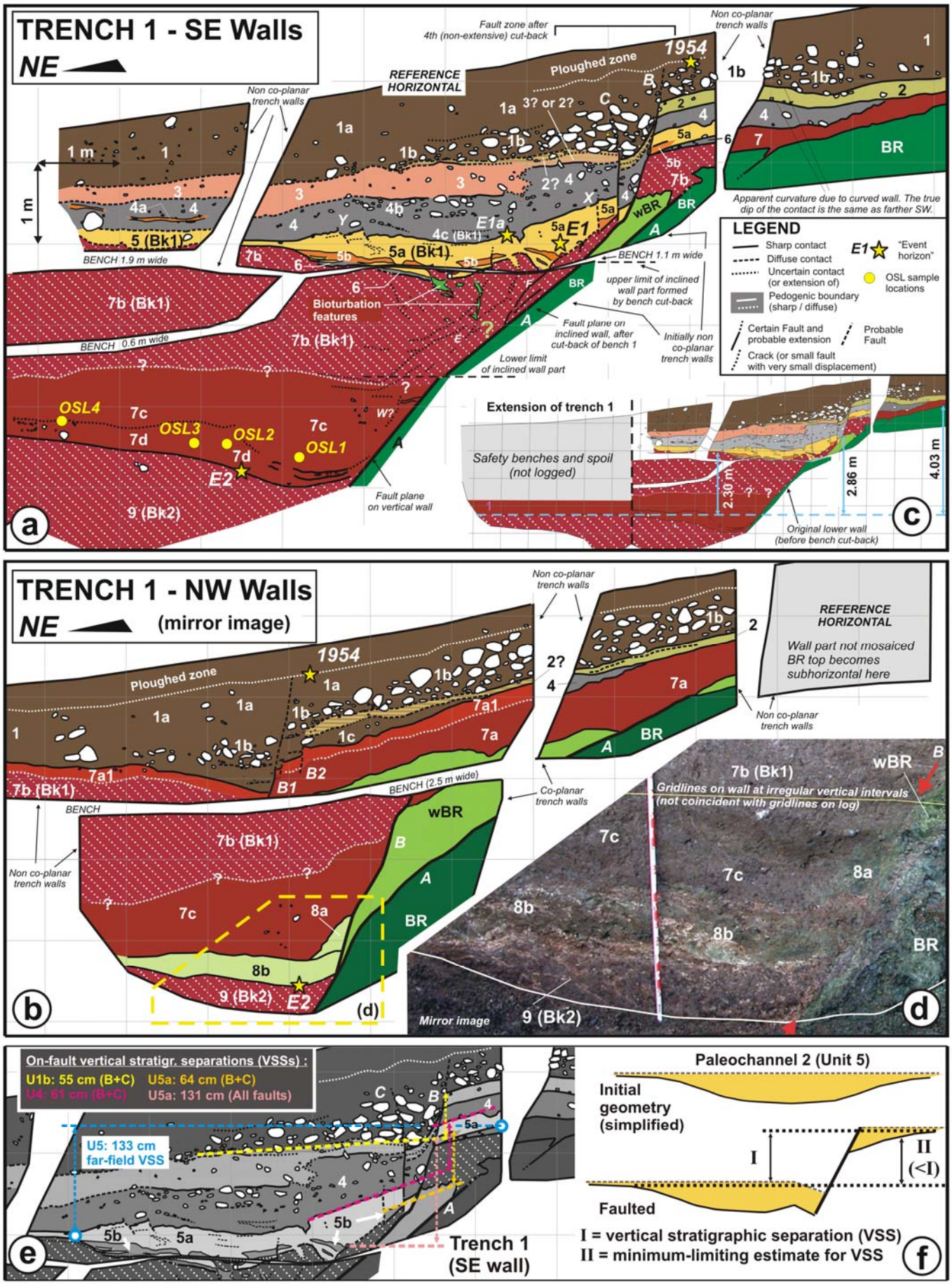

Figure 3. a/b: Logs of Trench 1 walls. Lithological units are described in Figure 4 (bottom). The lower part of the SE wall is shown after cut-back of the safety bench between it and the upper part of the wall. For safety reasons, the bench was cut-back to an inclined wall. **c:** SE wall after extension of bottom part. **d:** Unit 8, the debris element [*sensu Nelson*, 1992] of the scarp-derived colluvial wedge associated with paleoseismic event E2. **e:** Measurements of on-fault and far-field vertical stratigraphic separation (VSS) on the SE wall in T1. **f:** Simplified model to explain the measurement of the "far-field" VSS of paleochannel 2. The far-field measurement in (e) corresponds to "II" in (f).

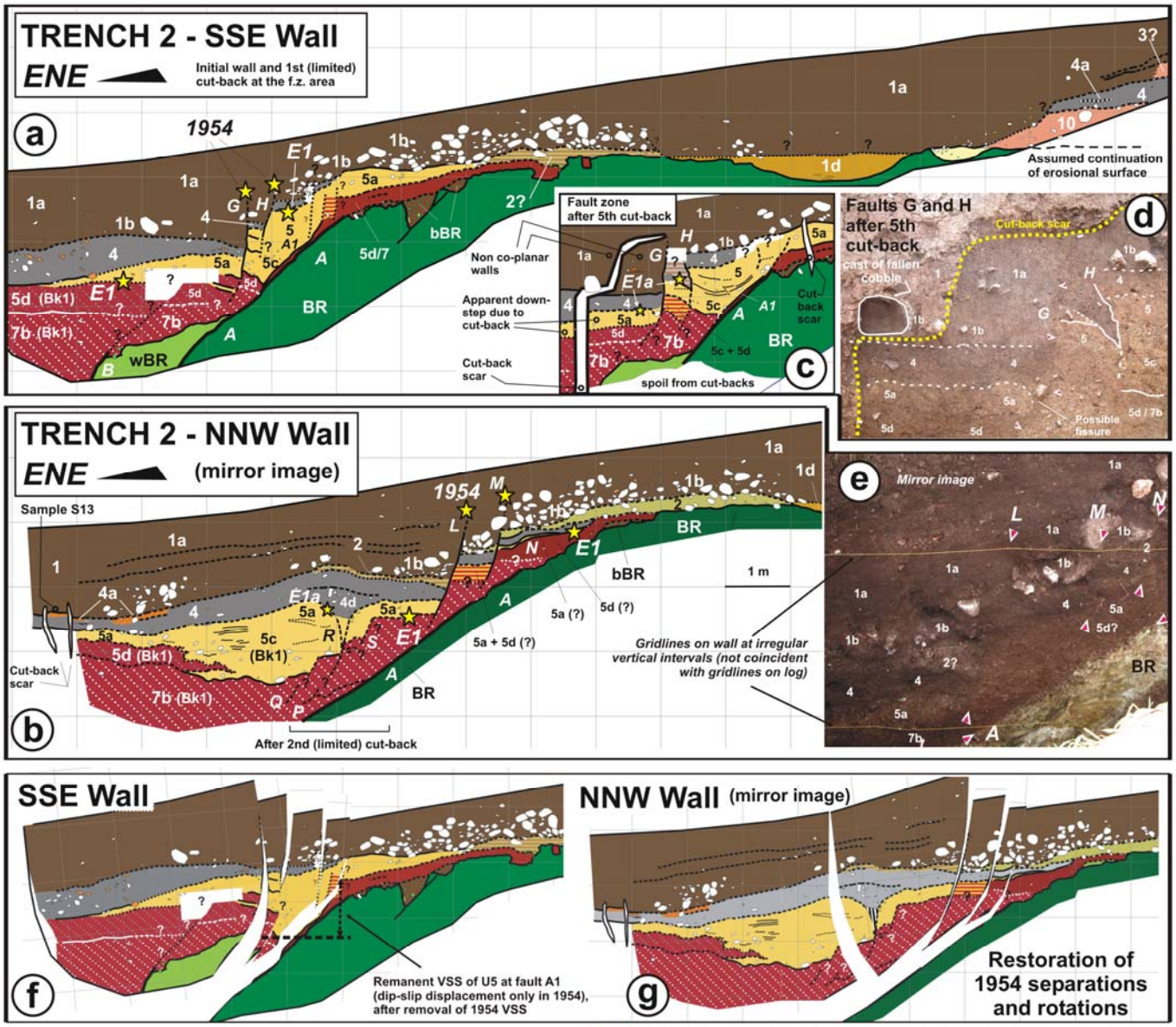

Description and interpretation of lithostratigraphic units in Trenches 1 - 3

[For descriptions of soil-stratigraphic features, see text]

1, 1d — Matrix: Dark brown silt / clayey silt with abundant, sparse angular clasts (predominantly < 5 mm). **1a/1c:** sparse large pebbles, and cobbles. Bedding is locally discernible in 1a on the downthrown fault block, corresponding to a horizon of relatively increased concentration of large clasts and ceramic fragments. **1b** contains abundant cobbles/small boulders, a lot of which are subrounded/rounded and come from non peridotite rocks (i.e. They do come from the slope lying to the SW of the trenches, which consists of peridotites). **1d** is typified by lighter-colored, coarser (sandier) matrix compared to the rest of U1, locally discernible clear lamination and fining-upwards grading. ***Interpretation:*** **1a / 1c:** colluvium (mixed perhaps with alluvial fan fines). **1b:** colluvium with material deriving from man-made ancient constructions (or, mudflow deposit?). **1d:** channel deposits

2 — Matrix: olive green to light brown silt. Contains abundant sand and subangular pebbles, grain size generally reducing from the base to the top of the unit. Locally, a distinct limit between a coarser lower part and a finer upper part is discernible. ***Interpretation:*** alluvial deposits from unchanneled surface flows.

3 — Matrix: Reddish beige silt / clayey silt with abundant, sparse angular clasts (predominantly < 5 mm in diam.). Contains very few, sparse cobbles and coarse gravel (2-6 cm diam.). ***Interpretation:*** colluvium

4 — Matrix: Gray to dark gray silt/clayey silt with abundant, sparse angular clasts (predominantly < 5 mm in diam.) and pieces of charcoal (absent or very rare in other units). **4a:** horizon rich in amorphous clay debris, underlain by a horizon characterized by much darker gray (almost black) matrix. **4b:** includes abundant large clasts (diam. up to 15 cm). **4c:** is characterized by horizontal lamination (laminae containing fine pebble-sized amorphous baked clay pieces and charcoal pieces in a matrix similar to the rest of the unit) and horizontal orientation of included ceramic sherd. Rich in $CaCO_3$ precipitates along lamination. **4d:** characterized by increased concentration of sherds and animal bone fragments, compared to the rest of U4 in T2. ***Interpretation:*** colluvium, derived from human occupation horizons a short distance uphill from the trenches (see text for archaeological content). **4b:** could be a man-made deposit. **4c:** colluvial material possibly reworked in paleochannel 2. **4d:** fissure fill, possibly man-made. The $CaCO_3$ precipitates within 4c, as well as elsewhere in the lower part of U4 indicate that it has been affected by calcic soil development (Bk1).

5, 5b, 5d — **5a:** light olive green to dark yellow silty sand / sandy silt, rich in subangular and angular peridotite clasts (1 to 4 mm diam.). Bedding and fining upwards grading discernible locally. Parts of 5a near the fault zone, in the uppermost part of paleochannel 2 are richer in reddish silt and completely lack bedding and grading. **5b:** reddish brown silt / silty clay and very fine / fine sand (fining upwards grading discernible locally). **5c:** as 5a, containing larger clasts. **5d:** reddish brown silt/clayey silt with abundant, sparse angular clasts (predominantly < 5 mm in diam.). Few, sparse larger angular clasts (2-4 cm in diam.). Lateral transition to 5c. ***Interpretation:*** **5a-c:** channel deposits (paleochannel 2). **5a:** includes also scarp-derived colluvium (originating from U5 and U7). **5d:** overbank fines of paleochannel 2. All of U5 has been affected by calcic soil development (Bk1).

6 — Similar to U4, only richer in sherds (generally larger than those typically found in U4) and charcoal pieces (larger than in U4). Affected by the formation of Bk1. ***Interpretation:*** colluvium derived from human occupation horizons lying very near by.

10 — Similar to U3. ***Interpretation:*** colluvium.

7 — Matrix: reddish brown silt /clayey silt with abundant, sparse angular clasts (predominantly < 5 mm in diam., but also up to 1-2 cm). **7a / 7c**: unit 7 without Bk1 development. 7a1 in T1 (NW wall) has a stronger red hue, suggesting stronger oxidation. **7b:** affected by Bk1 development. **7b1-3:** sub-units distinguished based on differences in Bk1 morphology (see text). **7d:** richer in larger, angular peridotite clasts (typically 3 cm or larger, up to 6-10 cm) compared to the rest of U7. A sharp upper limit or bedding are observed locally. ***Interpretation:*** colluvium (mixed perhaps with an unknown percentage of alluvial fan fines).

8 — **8a:** fine-pebble sized fragments derived from friable wBR. **8b:** In T1, closely packed large pieces of wBR, mixed with transported fines and $CaCO_3$ deposits originating from Bk2 on the upthrown block and, U7c material. In T3, wBR material and $CaCO_3$ deposits, transported as in T1, but also in situ (belonging to Bk1). ***Interpretation:*** debris facies colluvium derived from wBR and U9.

9 — Matrix: Same as U7. U9 has been subjected to calcic soil formation (Bk2). In T3 it contains well rounded, large pebbles and cobbles (predominantly peridotite). ***Interpretation:*** alluvial fan deposits mixed with colluvium.

wBR — Intensely sheared peridotite bedrock, with friable or "buttery" texture.

bBR — Regolith material, subjected to limited reworking as colluvium.

BR — Peridotite, rich in tectonic discontinuities and shear zones. Much harder/compact than wBR.

Figure 4. a/b: Logs of Trench 2 walls. **c:** Fault zone on the SSE wall after 5th cut-back. **d:** view of faults G and H (SSE wall) after 5th cut-back. **e:** view of faults L, M and N (NNW wall). **f/g:** restorations of the trench stratigraphy to its pre-1954 state. Unit descriptions for all trenches are given at the bottom of the figure.

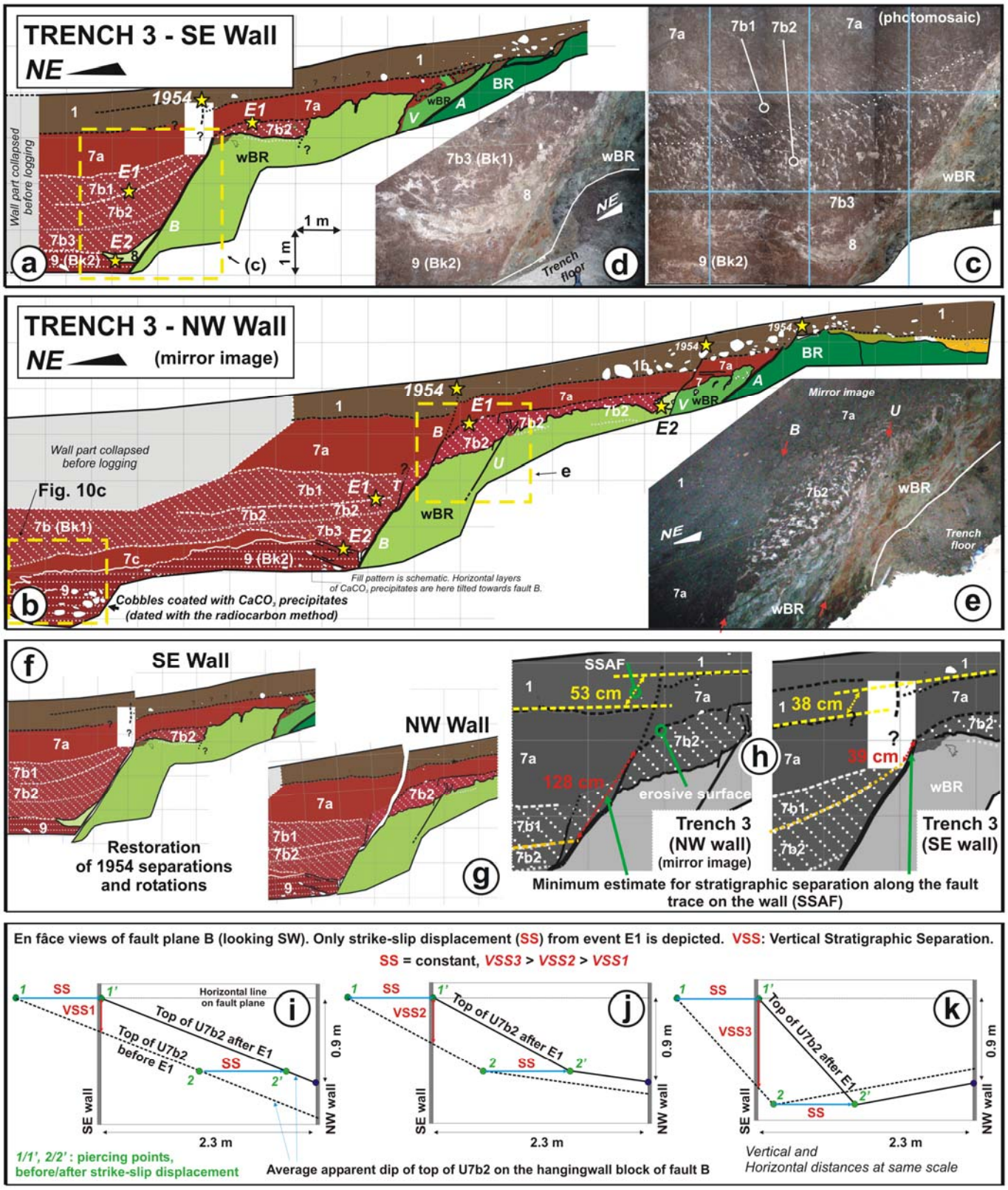

Figure 5. a/b: Logs of Trench 3 walls. **c:** fault B (SE wall). **d:** the scarp-derived debris wedge associated with event E2 (Unit 8, SE wall). **e:** faults B and U (NW wall). All photos (c-e) taken at nightfall with flash. **f/g:** restorations of the trench stratigraphy to its pre-1954 state. **h:** separation measurements on fault B. **i-k:** En face views of fault plane B, with graphs showing the effects that the horizontal component of displacement has on the vertical stratigraphic separation of the top of U7b2 on the downthrown block.

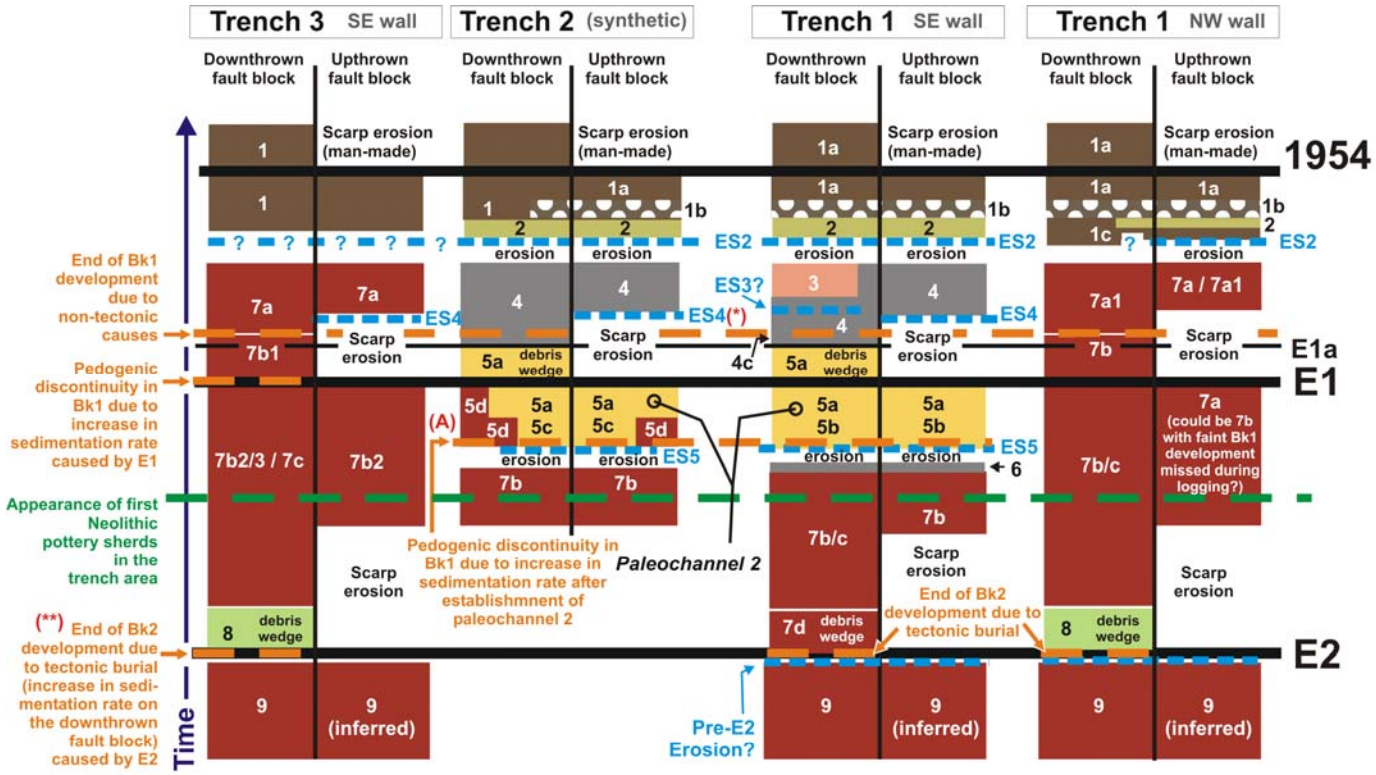

The time scale (vertical graph axis) is arbitrary, and the vertical extent of stratigraphic unit depictions is not proportional to the time it took for them to deposit. E.g. The fill of paleochannel2 (most of Unit 5), expectedly deposited much faster compared to the underlying U7b/c than the figure implies. Also, U8 expectedly deposited faster than U7d, but both are shown to have deposited in the same amount of time for simplification.

"Scarp erosion" refers to fault scarps formed by co-seismic ground ruptures. The graph refers to units within 2 m or less from the fault zone (on both the upthrown and downthrown block) [exception: (A) in Trench 2]. Those units that are distinguished by pedogenic boundaries that correspond to bases of soil horizons (e.g. U7b/7c in T1), are grouped here into the same chronostratigraphic unit, because the pedogenic boundaries that distinguish them post-date both the underlying and overlying stratigraphic unit. For simplification, upper boundaries of Bk horizons that are of pedogenic origin (the 7a/7b1 and the 7a1/7b boundary on the downthrown fault block in T3 and T1, respectively) are treated as if they were regular stratigraphic boundaries.

(*): This is one of the two alternative interpretations of the fault footwall stratigraphy on the SSE wall of Trench 2 (see Figure 8). (**): The line representing the end of Bk2 development due to tectonic burial would not be horizontal in this graph if all of the downthrown block was considered (and not just the near-fault area), due to progressive burial by lateral progradation of the E2 colluvial wedge [e.g., see *McCalpin and Berry*, 1996].

Figure 6. Chronostratigraphic correlation of lithostratigraphic units in the trenches. Paleoseismic events, events pertaining to soil formation, and the appearance of first Neolithic ceramic sherds are also noted as time markers.

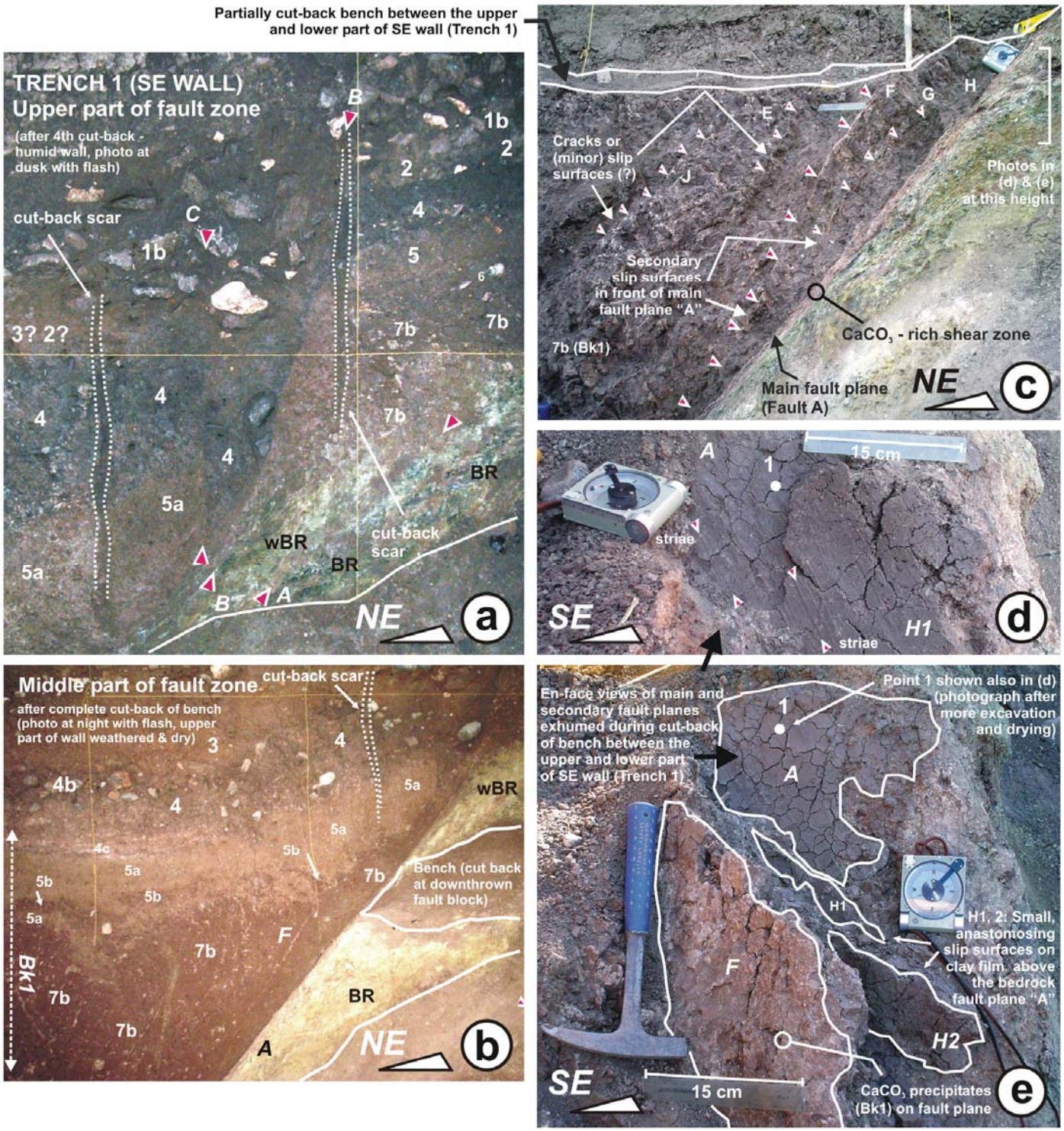

Figure 7. **a:** View of the upper part of the fault zone and stratigraphic units in Trench 1 (T1, SE wall). Arrows point to splays of the fault zone (not traced on photograph). **b:** View of the middle part of the fault zone and stratigraphic units, after complete cut-back of the bench between the upper and lower parts of the SE wall of T1. **c:** View of the middle part of the fault zone, during bench cut-back (irregular –not flat- wall), and of the discontinuities (fault splays and cracks, indicated by arrows, not traced on photo) and pedogenic $CaCO_3$ deposits accumulated along them. **d and e:** En fâce views of fault planes exhumed during bench cut back [location in (c)]. Arrows in (d) indicate striae (not traced on photo) on clay film over the main fault plane and on small secondary splay right in front of it. $CaCO_3$ accumulations on fault F are also discernible.

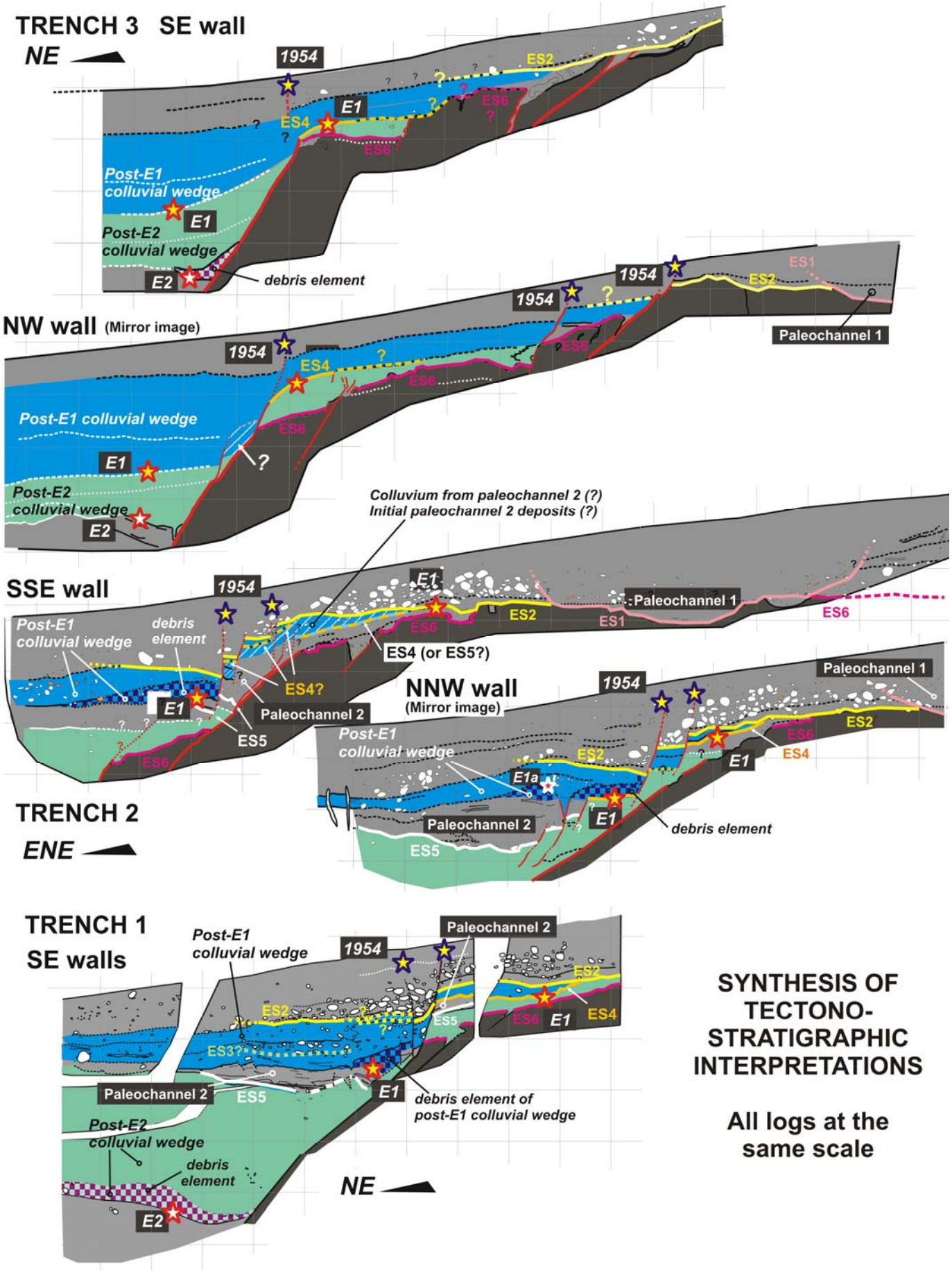

Figure 8. Interpretation of trench logs. Stars indicate event horizons of slip and cracking events. ES1 to 6: erosional surfaces 1 to 6. See text for discussion.

Figure 9. Characteristic archaeological material found in trenches 1 and 2, with brief descriptions, from *Froussou* [in press]. **a:** sherds from vessel broken *in situ* (sample S13). **b:** vessel parts, reconstructed from sherds in (a). **c:** View of the sherd-rich unit 4 (U4). Sherds are indicated by yellow dots next to (or, on) them. **d:** a large, well-preserved vessel fragment within U4. **e:** Large sherd from U4. **f:** Sherd with painted decoration from U5. **g:** Sherds within U6 and U7b.

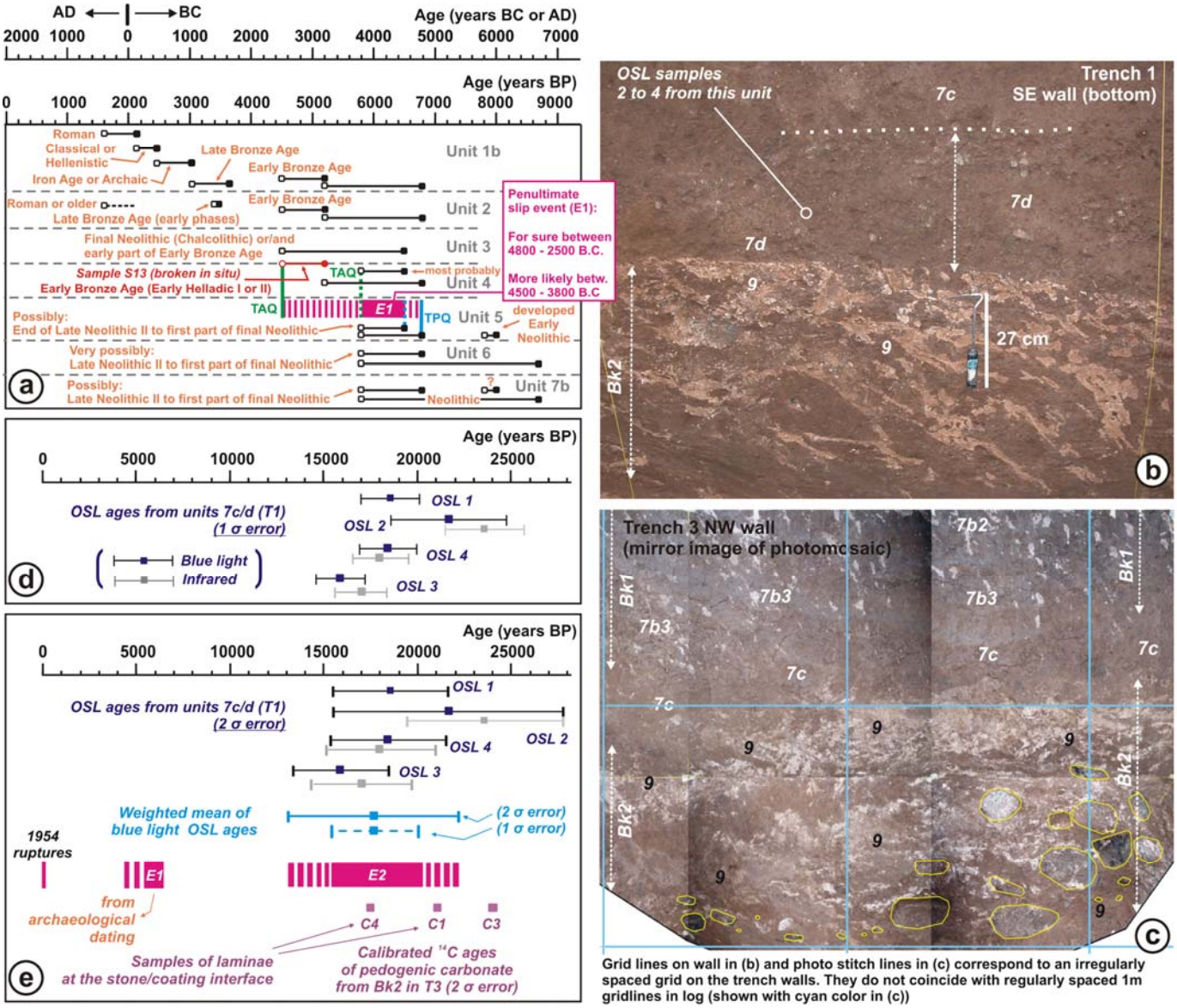

Grid lines on wall in (b) and photo stitch lines in (c) correspond to an irregularly spaced grid on the trench walls. They do not coincide with regularly spaced 1m gridlines in log (shown with cyan color in (c))

Figure 10. a: Graphical summary of ages of transported sherds in trenches 1 and 2, and constraints on the timing of the penultimate event of 1954-like slip (E1). **b:** Close-up view of U7d and its very sharp lower boundary with U9 and Bk2 (T1 SE wall). OSL samples 2 to 4 come from unit 7d. **c:** view of Bk2 (unit 9) and of the vertical distance between its upper boundary and the lower limits of Bk1 at the distal part of T3 (NW wall), where sampling of stone coatings of pedogenic carbonate was conducted. **d:** OSL ages from units 7c/d (1 σ error). **e:** OSL ages (2 σ error) and their weighted mean, and ^{14}C ages of pedogenic carbonate from Bk2 in T3 (except for the age of sample C2, which is not calibratable).